ABSTRACT

The dose distribution around brachytherapy (BT) sources is characterized by steep dose gradients and an energy spectrum varying rapidly with depth in water around the source. These two properties make experimental verification of the dose distribution difficult, and put high demands on the dosimetry system in use regarding precision, size and energy dependence. The American Association of Physicists in Medicine (AAPM) recommends lithium fluoride (LiF) thermoluminescence dosimetry (TLD) to be used for verification measurements, as it is the only dosimetry system meeting the requirements, but still the total combined uncertainty in dose-rate determination is as high as 7-9 % (1 σ). Lithium formate is a new dosimetry material that is less energy dependent than LiF, but more sensitive than the most common EPR (electron paramagnetic resonance) dosimetry material, alanine. In order to evaluate lithium formate EPR for BT dosimetry, dosimeters were produced for experimental dose determination around BT source ^{192}Ir. The dosimeters were calibrated against an ionization chamber in a high energy photon beam. Dose to water was determined at 1, 3 and 5 cm radial distance from the source, which was stepped along a straight line in a PMMA phantom. The experiments were performed twice using 4 dosimeters per distance and experiment. Methods to correct for energy dependence were developed and evaluated. The uncertainty in measured dose was estimated. The experimental dose values agreed with the values from the treatment planning system with a maximum deviation of 3.3 %, and an average 1 σ uncertainty of 3 % at 3 and 5 cm and 5 % at 1cm. Uncertainty in radial distance from the source as well as source calibration were the dominating contributions to the total combined uncertainty. Lithium formate EPR has been shown to be a promising alternative to LiF TLD for BT dosimetry.

1 INTRODUCTION

Before a new brachytherapy (BT) source model can be used clinically, its dose distribution must be well characterized, both experimentally and by Monte Carlo (MC) calculations. The American Association of Physicists in Medicine (AAPM) recommends the BT dose calculation formalism presented in the Task Group 43 (TG-43) report (Rivard et al 2004) to be used in all treatment planning systems (TPS). The report gives instructions how to measure the dose-rate in water around BT sources together with a formalism for dose calculation and data sets of parameters determining dose distribution derived from a combination of MC calculations and experimental results. The parameters are entered into TPS.

The derivation of experimental data in BT dosimetry is equipped with some difficulties. Steep dose gradients, a wide range of doses, low photon energies (20-800 keV) and a wide energy spectrum, which changes with depth, are some characteristics that complicate dose measurements and put high demands on the dosimetry system in use. Typically the combined 1 σ uncertainty (k = 1, 67 % confidence index) in the experimental data lies around 8 % (Thomadsen et al 2005). It would be of great interest to reduce this uncertainty.

The uncertainty can be held low by accurate detector positioning and by minimizing detector dose-rate dependence, dose response nonlinearity, energy dependence, volumetric averaging, temporal stability of readings and calibration coefficients (Rivard et al 2004). Among the methodological recommendation of the TG-43 report the detector used for measurements of BT dosimetry parameters should be small enough for effects of volume averaging to be negligible or accurately corrected for, a well-characterized energy-response function and sufficient precision and reproducibility to allow dose-rate estimation with 1 σ Type A uncertainties $\leq 5\%$, and 1 σ Type B uncertainties < 7% (Rivard et al 2004).

Lithium fluoride (LiF) thermoluminescence dosimetry (TLD) is currently the recommended method for experimental determination of the dose distribution around BT sources. It is the only dosimetry system that has been convincingly demonstrated to be suitable for this purpose, thanks to its high sensitivity (Rivard et al 2004).

Lithium formate is a material that can be employed for dosimetry by using electron paramagnetic resonance (EPR) spectroscopy for signal read out. Studies have recently shown that lithium formate has dosimetric properties that could match the requirements of a detector for measurements around BT sources. It has a higher sensitivity than the most commonly used EPR dosimetry material, alanine, low energy dependence and absorption characteristics similar to water, which is the recommended reference material by the TG-43.

^{192}Ir is a common BT source, used in the treatment of several forms of cancer. Its dose distribution is rather complicated to measure, since it possesses most of the typical characteristics of a BT source mentioned above. It is therefore a suitable source for the evaluation of a new dosimetry system such as lithium formate EPR.

The aim of this work was to evaluate the lithium formate EPR dosimetry system for measurements around ^{192}Ir BT source qualitatively and experimentally, by measuring dose at three different distances from the source and comparing the results with values given by the TPS. As the type of dosimeters used in this work never had been used for BT dosimetry before, methods to estimate and correct for energy dependence had to be developed.

2 THEORY

2.1 ^{192}IR BRACHYTHERAPY SOURCE

^{192}Ir is one of the most commonly used BT sources. With a half-life of 73.8 d and mean energy of approximately 350 keV it is suitable for the treatment of many cancer types using the afterloading technique for dose delivery to the tumor. The experimental characterization of the dose distribution around the source can be problematic though,

due to some of its properties. It has a wide spectrum of photon energies, ranging from 0.136 to 0.885 MeV. Photons of lower and higher energies than those in the stated interval are emitted by the radioisotope, but can be neglected in this context. This spectrum changes rapidly with distance from the source in water (**Figure 1**). The demands on the detector to be as energy independent as possible are thus high. Electrons are stopped in the encapsulation of the source and do not contribute to the dose to the patient.

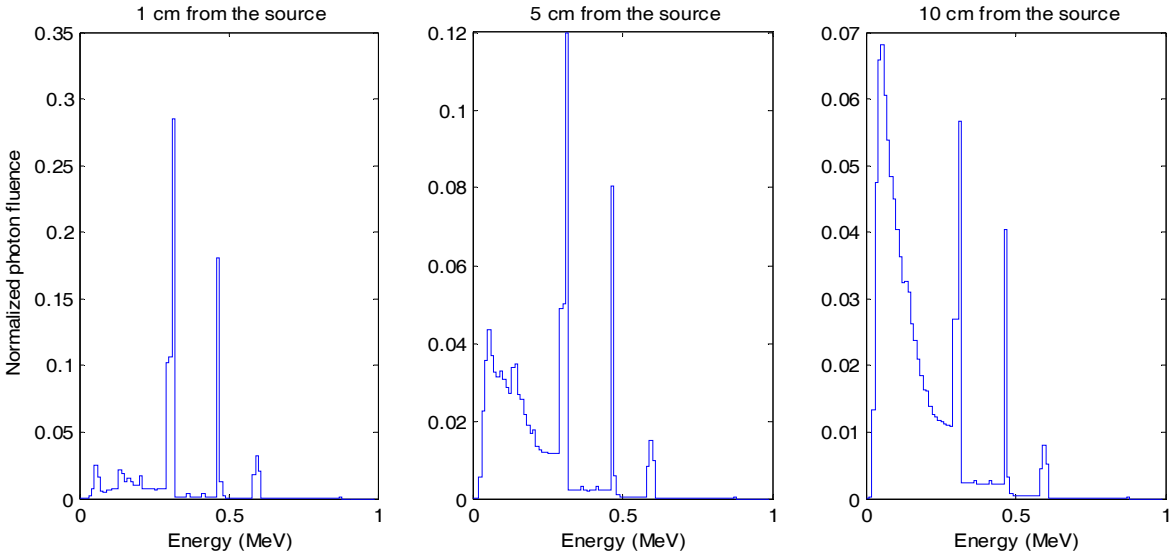

Figure 1 ^{192}Ir photon energy spectrum in water at 1, 5 and 10 cm radial distance from the source. The spectra have been derived by EGS4 MC simulations in conjunction with calculations around a mHDR-classic ^{192}Ir source (Carlsson Tedgren , personal communication).

2.2 DOSIMETRIC PROPERTIES OF LITHIUM FORMATE

When lithium formate monohydrate (HCO_2 Li H_2O) is irradiated by ionizing radiation, free radicals of two types are produced (Vestad et al 2004 a). The amount of produced radicals corresponds to a certain dose and can be measured using the technique of EPR spectroscopy.

A free radical is an atom, molecule or ion with an unpaired electron. The production of the dominating radical produced in lithium formate, $\dot{C}O_2^-$, is described by the following equations

$$HCO_2^-Li^+ \xrightarrow{h\nu} HCO_2Li^+ + e^-$$

$$HCO_2Li^+ \longrightarrow \dot{C}O_2^-Li^+ + H^+$$

where the dot indicates a free radical (Vestad et al 2004 a).

Fading. In most materials free radicals are very reactive. In lithium formate, the radicals are prohibited from further reactions, due to the crystalline structure of the material. This property makes it possible to measure the radiation dose a long time after irradiation. The free radicals are not entirely stable though, and signal fading is a possible result if the dosimeters are stored for a long time between irradiation and read out. According to a recent study the EPR signal of lithium formate remains unchanged one week after irradiation to 10 Gy, if the irradiated samples are stored under normal environmental conditions (Vestad et al 2003). The fading characteristics of lithium formate must be investigated systematically though.

Dose response linearity. Lithium formate exhibits no zero-dose signal and shows a linear dose response between 0.2 to 1000 Gy (Vestad et al 2003). This is an advantage compared to LiF that is supralinear above a certain dose level (Vestad et al 2004 b). Corrections for supralinearity add some uncertainty to the dose calculations and should be avoided if possible.

Sensitivity. Compared to alanine, which is the standard EPR dosimetry material, lithium formate is stated to be 2-7 times as sensitive (Vestad et al 2003). This property makes it possible to produce small dosimeters that are required in the steep dose gradients around BT sources. High sensitivity is also crucial for the precision in dose determination.

Water equivalence. Since the TG-43 recommends water as reference material for BT treatment planning, it is advisable that the dosimetry material is as water equivalent as possible. One aspect of water equivalence is the effective atomic number, Z_{eff}, which for lithium formate is closer to water than both alanine and LiF (**Table 1**). The density of the active material lithium formate is 1.48 g/cm^3 compared to water that has a density of 1.00 g/cm^3, while LiF has a higher density than lithium formate (**Table 1**). The dosimeters used in this work contain 10 % paraffin which gives a dosimeter density of 1.27 g/cm^3. See Section 3.1. The equivalence to solid phantom materials, such as polymethyl methacrylate (PMMA), that are often used to substitute water for the sake of positional accuracy in experiments, is a related requirement which lithium formate meets well as PMMA has a density of 1.19 g/cm^2. The similarity in density highly reduces dosimeter perturbation effects in the phantom.

Table 1 Effective atomic number and density of water and the dosimetry materials lithium fluoride, alanine and lithium formate. (Vestad 2004)

	Water	**LiF**	**Alanine**	**Lithium formate**
Effective atomic number	7.5	8.3	6.8	7.3
Density (g/cm^3)	1.00	2.64	1.45	1.48

Due to its high water equivalence, lithium formate has similar radiation absorption characteristics as water. More important for dose measurements around BT sources, is that the ratio of mass energy absorption coefficients between the dosimeter material and water, $(\mu_{en}/\rho)_{dosimeter}/(\mu_{en}/\rho)_{water}$, has a low energy dependence (**Figure 2**). This is true to an even higher extent for the ratio of mass collision stopping power between the dosimeter material and water, $(_{m}s_{coll})_{dosimeter}/(_{m}s_{coll})_{water}$, (**Figure 3**). Such an independence of energy makes the knowledge of the local photon energy spectrum less critical, which reduces a great source of uncertainty in BT dose measurements.

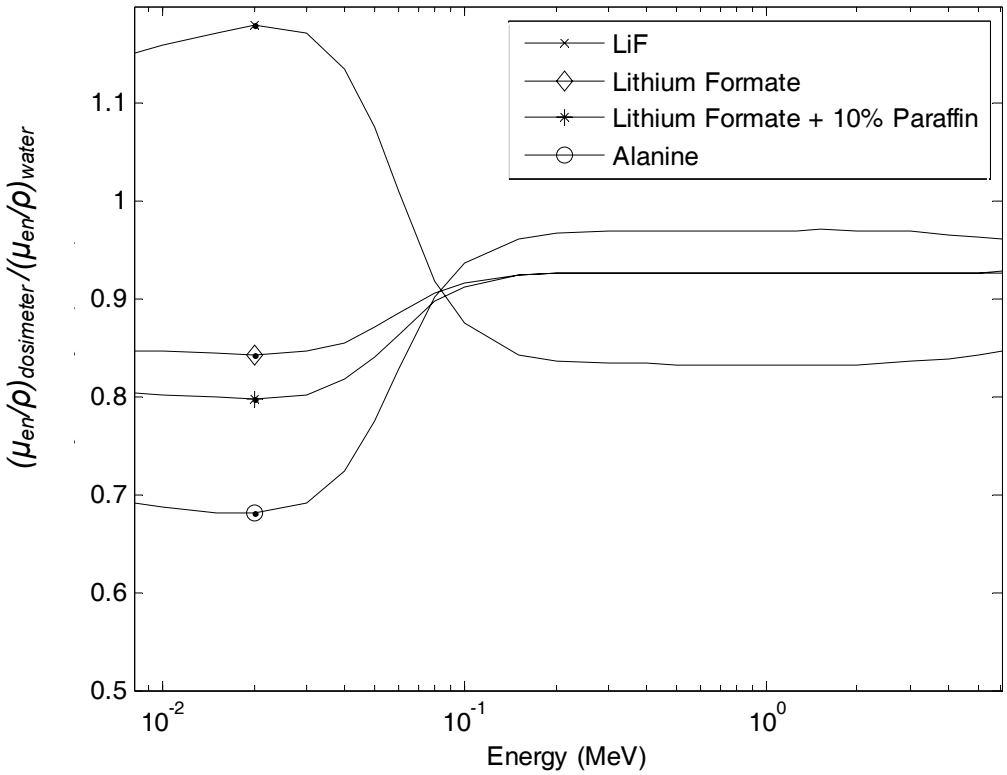

Figure 2 Mass energy-absorption coefficient ratios between different dosimetry materials and water. 10 % paraffin was used as a binder in the dosimeters of this work, which is the reason why its absorption coefficient ratio is displayed in the figure.

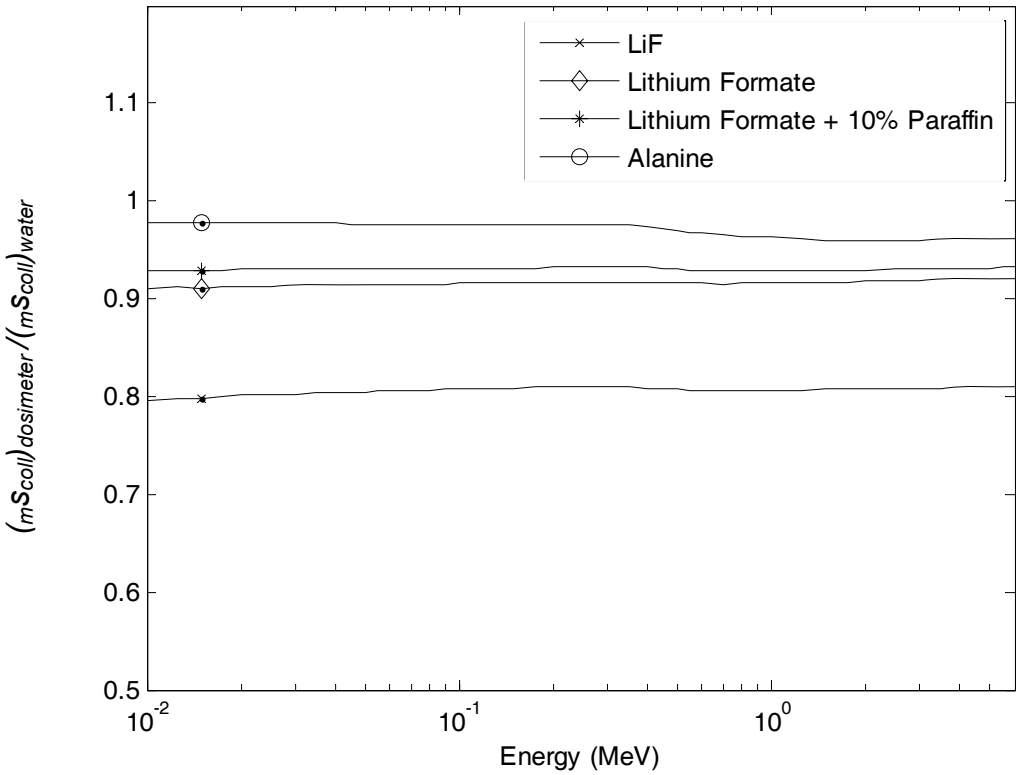

Figure 3 Mass collision stopping power ratios between different dosimetry materials and water. 10 % paraffin was used as a binder in the dosimeters of this work, which is the reason why its stopping power ratio is displayed in the figure.

Energy dependence. As mentioned above, a low energy dependence of the dosimetry system for BT sources is desirable, since the energy spectrum often varies from point to point in the measurement geometry around the source. The uncertainty in the relative energy response correction, *E(r)*, defined as the ratio of dosimeter response per unit dose in water at the measurement point in the BT geometry to the response per unit dose in the calibration geometry, often dominates the total dose uncertainty (Rivard et al 2004). Energy response artifacts could include volume averaging, self absorption, medium displacement and differences between the phantom material and water, as well as intrinsic energy response according to TG-43. Recent measurements have shown very low energy dependence for lithium formate in electron beams of energies between 6-20 MeV and a ^{60}Co reference field (Malinen et al 2007). This should hold for lower energies too, due to the high water equivalence of lithium formate and due to the rather constant mass energy-absorption ratios compared to other dosimetry materials used for similar

applications. Dose response measurements in X-ray qualities (60 kV - 220 kV) compared to ^{60}Co by Vestad et al (2003) confirm the assumption of low energy dependence. Because of the high sensitivity of lithium formate compared to alanine, relatively small dosimeters can be produced, which reduces the effects of volume averaging.

These properties all make lithium formate a good candidate for dose measurements around BT sources.

2.3 EPR SPECTROSCOPY

Spectroscopy is the measurement and interpretation of energy differences between different atomic or molecular states. The following section will give a brief introduction to the basic physics, on which the EPR measurement of radicals depends and a short comparison of the EPR read-out technique with the TLD read-out technique.

All electrons have a magnetic moment, μ, and a spin quantum number, $S = 1/2$. In an external magnetic field, B_0, the magnetic moment aligns itself either parallel or anti-parallel to the field, giving rise to two possible energy states, $m_s = \pm 1/2$. The parallel state ($m_s = -1/2$) is of lower energy, and the anti-parallel state ($m_s = +1/2$) is of higher energy. The energy of a state is in the simplest case proportional to the magnetic field according to

$$E = m_s \, g \, \mu_B \, B_0 = \pm 1/2 \, g \, \mu_B \, B_0$$

where g is the gyromagnetic ratio and μ_B the Bohr magneton. The difference between the two energy states is thus

$$\Delta E = E_{+1/2} - E_{-1/2} = g \, \mu_B B_0$$

The relationships are illustrated in **Figure 4** (Weil, Bolton and Wertz 1994).

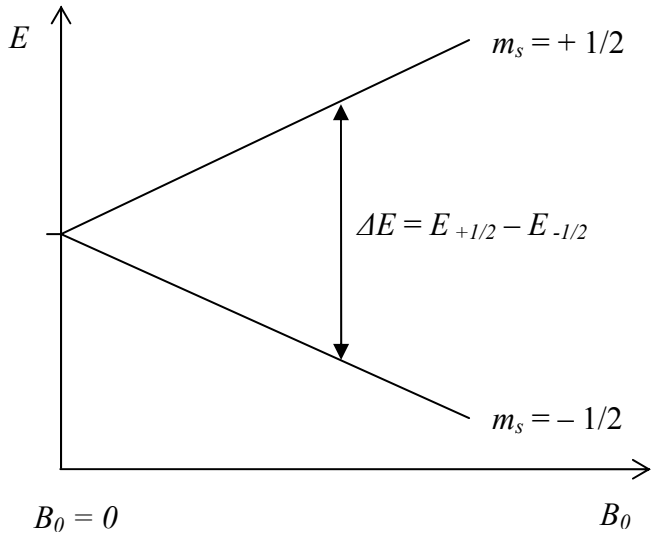

Figure 4 The separation of the energy states with increasing magnetic field, B_0.

The unpaired electron of a free radical can switch between the two energy states if electromagnetic (EM) radiation of energy $h\nu = \Delta E$ is either absorbed or emitted. In an EPR spectrometer the sample is irradiated by EM radiation of constant frequency, while the magnetic field is scanned. The energy difference ΔE between the spin states will slowly increase with increasing B_0, until it matches the energy ε of the EM radiation. Since there are more unpaired electrons in the lower energy state there will be a net absorbance of energy.

The electrons in a sample experience slightly different magnetic fields, e.g. due to hyperfine interactions between neighboring particles producing local magnetic fields. Since the absorbance peak is a superposition of many components, the hyperfine interactions lead to a broadening of the curve, that approaches a Gaussian shape. The peak-to-peak amplitude of the first derivative of the absorbance peak is used as a quantitative measure of the amount of free radicals in a sample (**Figure 5**). The absorbance is described by the equations in **Table 2**.

Table 2 Gaussian equation describing the absorbance of electromagnetic radiation by a sample containing free radicals, its derivative and peak-to-peak amplitude.

Property	**Equation**
Absorbance equation	$Y = Y_{\max} \exp\left(\frac{-\ln 2\,(B - B_r)^2}{\Gamma^2} \right)$
Peak amplitude	$Y_{\max} = Y\big\|_{x=x_r} = \sqrt{\frac{\ln 2}{\pi}} \frac{1}{\Gamma}$
Half-width at half-height	$\Gamma = \frac{1}{2} \Delta B_{1/2}$
First-derivative equation	$Y' = -Y_{\max} \frac{2 \ln 2 (B - B_r)}{\Gamma^2} \exp\left(\frac{-\ln 2\,(B - B_r)^2}{\Gamma^2} \right)$
Peak-to-peak amplitude	$2Y'_{\max} = 2\sqrt{\frac{2}{\pi e}} \frac{\ln 2}{\Gamma^2}$

Read-out. Dosimeters used in combination with the EPR read-out technique cannot be re-set since the radicals remain in the sample after read-out. Compared to LiF TLD this is a disadvantage regarding workload, but an advantage regarding read-out precision, which can be increased by increasing the number of read-out scans. The signal of LiF TLD is erased during read-out, which means that the signal can be obtained only once.

The precision of the EPR read-out technique is somewhat worse than of TLD though. Vestad et al performed a comparative study between lithium formate EPR and LiF TLD (2004 b) and found that the average relative standard deviation in dosimeter reading per dose is three times higher for lithium formate EPR than for LiF TLD at low doses about 0.5 Gy. Above 2.5 Gy though, the read out precision is approximately the same for both dosimetry systems. Since the dose levels are not critical in BT source verification measurements, doses above 2.5 Gy can be chosen to improve precision.

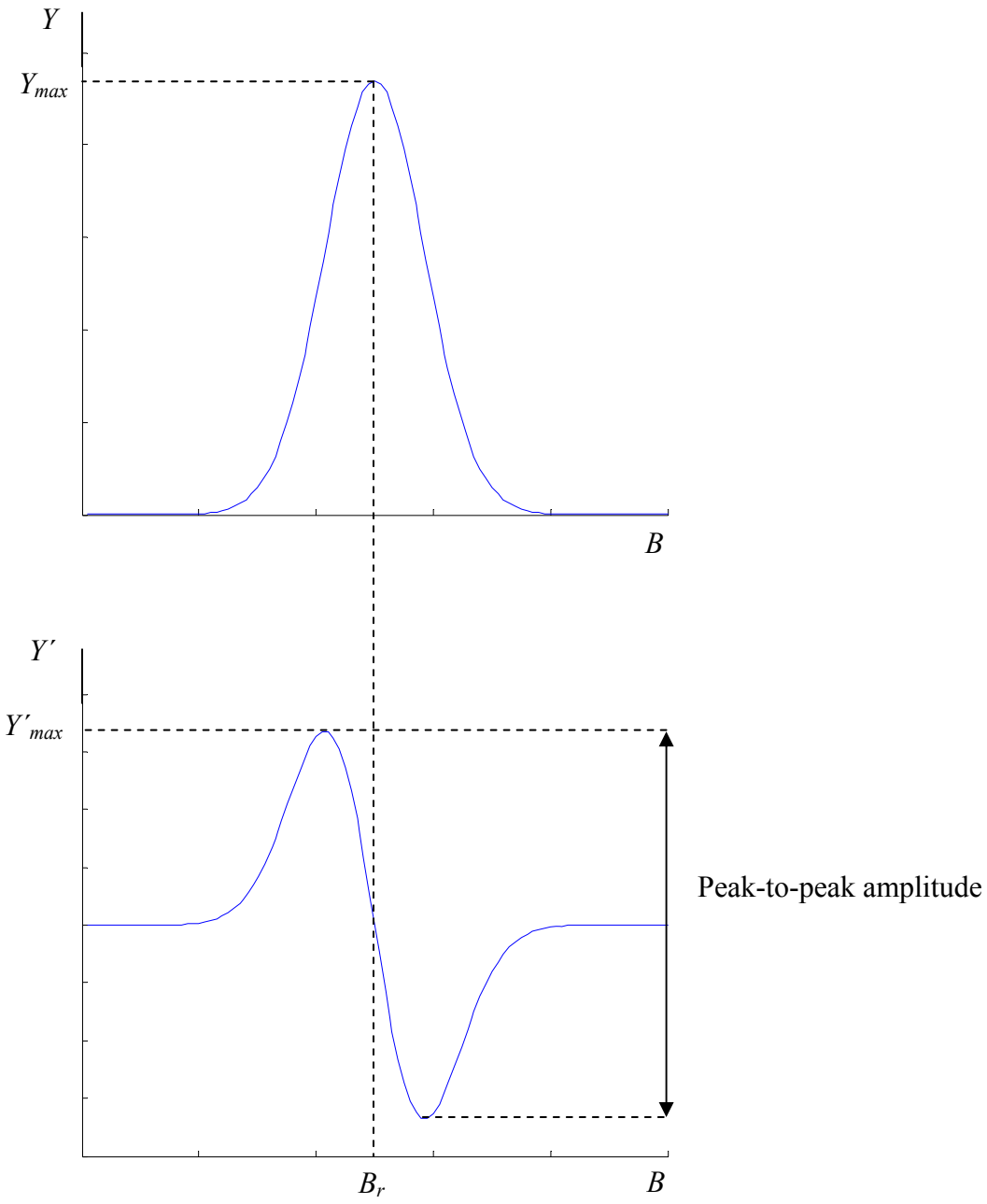

Figure 4 Absorbance, Y, of electromagnetic radiation in a sample and the first derivative, Y', of the absorbance. Theoretical example.

2.4 THE LITHIUM FORMATE EPR DOSIMETRY SYSTEM

The dose determination procedure using lithium formate EPR is based on the general EPR dosimetry method described by Bergstrand et al (1998). Gustafsson (2008) has adapted the method to lithium formate EPR dosimetry. It is a secondary dosimetry method, since the dosimeters must be calibrated against a reference detector, but it is used for absolute dose determinations.

To measure dose with lithium formate, a whole batch of dosimeters is required, consisting of typically 20 dosimeters from the same production. The homogeneity of the batch is controlled by irradiating all dosimeters to the same dose, D_0'. The resulting signal should have a certain maximum spread for the batch to be accepted. The EPR signal, l_w, is defined as the peak-to-peak amplitude of the first derivative of the absorbance peak l (see Section 2.3) divided by the dosimeter mass, w. The batch is divided into a minimum of three groups; two for calibration curve determination and one for dose measurements.

The two groups of calibration dosimeters correspond to the two points necessary to establish a calibration curve (**Figure 6**). Only two points are necessary, since the dose response is linear in a sufficiently wide dose interval. See section 2.2. One of these groups is irradiated to an additional dose, D_1, giving a signal, $\overline{l}_w^1$, which is an average from all dosimeters of that group. The other group is not further irradiated. Instead its average signal can be regarded as background signal at zero dose (D_0 = 0) and is denoted $\overline{l}_w^0$. The calibration curve is thus given by

$$l_w = aD + \overline{l}_w^0 \qquad (1)$$

where a is the slope of the curve and D is the dose.

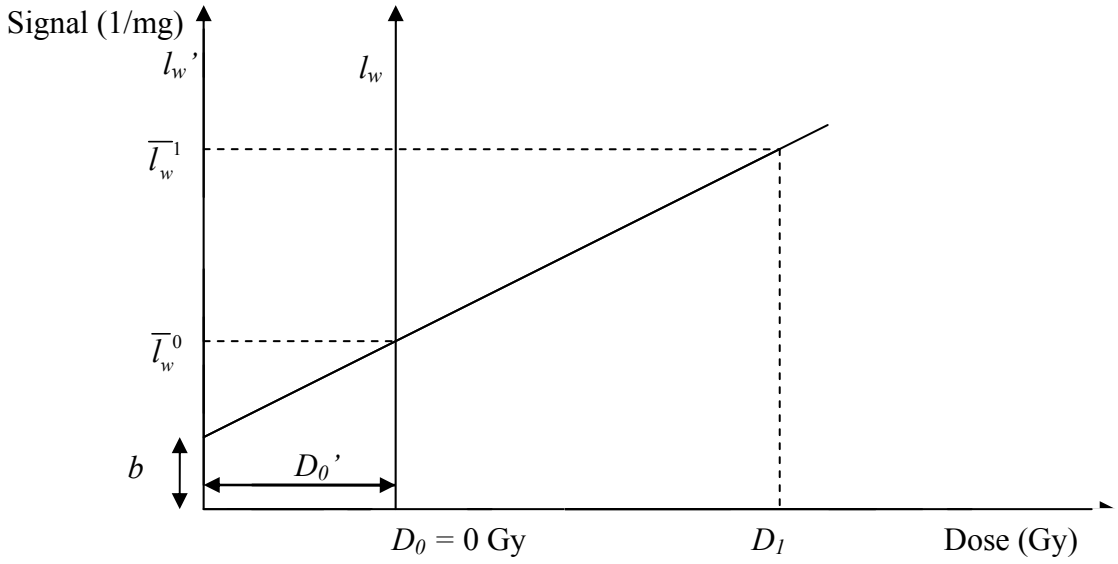

Figure 5 The calibration curve. The primes indicate that the symbols correspond to the former coordinate system. The symbols with no primes correspond to the new coordinate system in which the pre-irradiation dose, D_0', has been set to zero.

The remaining dosimeters of the batch can be used for dose measurements. To achieve optimal accuracy it is important that the dose, D_1, given to the calibration dosimeters, is higher than the dose, D_M, given to the measurement dosimeters. D_M is given by the following equation, which is a simple re-write of equation 1 with an additional correction term adapted to the measurement situation in this work,

$$D_M = (l_w - l_w^0)\frac{1}{a}\prod_j k_j \qquad (2)$$

where the k_i's are the correction factors that account for differences between the calibration situation and the dose measurement situation. The quantitative assessment of these factors is described in section 3.7.2. The mathematical treatment of the calibration curve is described in detail in section 3.7.1 and the uncertainty analysis in section 3.7.3.

3 MATERIALS AND METHODS

3.1 DOSIMETER MANUFACTURING

Gustafsson (2008) has developed a method of manufacturing lithium formate dosimeters for use in high energy photon beams. In the beginning of the present work an attempt to produce dosimeters smaller than the standard size was made, but resulted in very fragile dosimeters. In order to strengthen the dosimeters an increased amount of binding material was added, which reduced the sensitivity to levels that would require unreasonably long irradiation times. Thus the relatively large standard dosimeter size (5 mm height) was used for the measurements around ^{192}Ir, even though low BT energies require smaller dosimeters.

Polycrystalline lithium formate monohydrate (98 %) (HCO_2 Li H_2O) from Aldrich is the active dosimetry material. Solid paraffin (C_nH_{2n+2}, n = 20 - 40) from Carbona AB is used as a binder. The dosimeters consist of lithium formate to 90 % of their weight and of paraffin to 10 %.

To achieve a lithium formate crystal grain size appropriate for dose measurements, two strainers are used (Endecotts MINOR) with grid sizes of 180 and 500 μm. The remaining powder is weighted to determine the amount of paraffin to be added. The two components are put together in a beaker. The beaker is heated in an oven to a temperature well below the melting point of lithium formate (94° C), but above the melting point of paraffin (54° - 56° C); so that the binder melts before lithium formate crystals are damaged. When the paraffin is completely molten, the two components are mixed thoroughly. The heating and mixing is repeated twice, whereupon the mixture is cooled to room temperature. 100 mg of the mixture is used to press cylindrical dosimeters of 4.5 mm diameter and 5 mm height in a pellet press (Parr instrument company) (**Figure 7**).

Figure 6 Four dosimeters constituting a typical group.

The dosimeters are weighted after being pressed. Dosimeters of the same mixture are regarded as belonging to one batch and are used together in the following experiments. A maximum mass difference of ± 2 mg was tolerated. Dosimeters outside these mass limits were excluded from the batch. The dosimeters are identified by being labeled in the following order: aI-aV, bI-bV, …, LI-LV. The dosimeters of one batch are all stored under the same environmental conditions to avoid EPR signal differences caused by other sources than ionizing irradiation.

3.2 BATCH HOMOGENEITY CONTROL

It is important that the dosimeters respond equally to irradiation. Since the dosimeters are handmade, variations in relative amount of lithium formate versus paraffin are possible and could affect sensitivity. The homogeneity of a batch was controlled by pre-irradiating all dosimeters to the same dose, D_0'. To achieve sufficient precision, it is important that the dosimeters are given a dose above 2.5 Gy (Vestad et al 2004). It is not critical though exactly which dose they are given, as long as all dosimeters get the same, since the signal l_w^0 will correspond to zero-dose.

A plastic phantom of 5x20x20 cm^3 was used (**Figure 8**). Ten dosimeters were irradiated simultaneously to D_0' = 3 Gy at 5 cm depth in a field of 15x15 cm^2 and Source to Skin Distance (SSD) of 100 cm by 6 MV photons (**Figure 9**). To achieve a depth of 5 cm, additional slabs of PMMA were placed on top of the phantom.

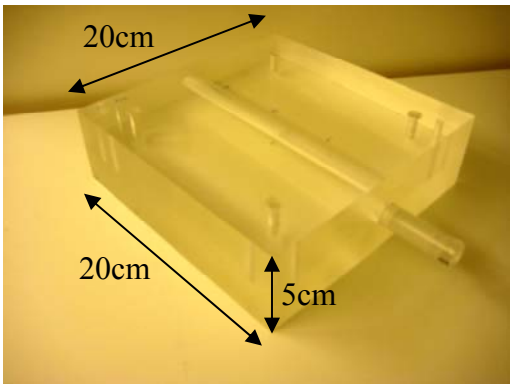

Figure 7 Phantom used for the pre-irradiation and for the calibration against an ionization chamber.

After the pre-irradiation the EPR signal of the dosimeters was acquired. For details, see section 3.3. If the relative standard deviation of the read-out signal, l_w, of one batch was less than 1%, the batch was accepted for further measurements. To reach this requirement, dosimeters with a signal deviating too much from the batch signal average were removed.

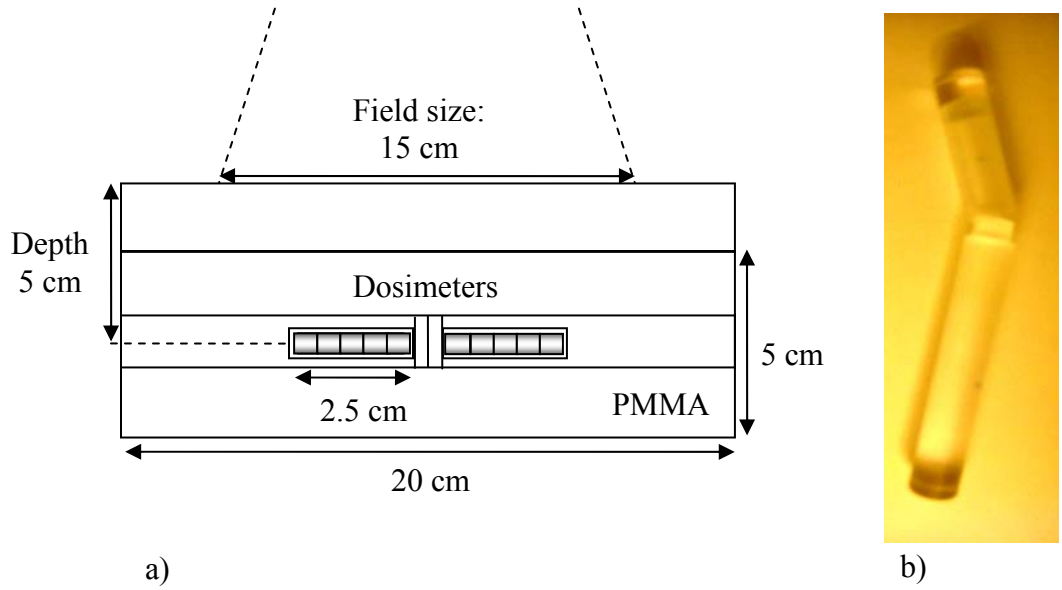

Figure 8 a) Set-up of the pre-irradiation of the dosimeters for the homogeneity control. b) PMMA holder for the dosimeters used in the pre-irradiation and in the calibration situation. Not to scale.

3.3 EPR READ OUT

The dosimeter signal was acquired using a BRUKER EleXsys E 580 EPR spectrometer equipped with a standard cavity ER 4102ST at Linköping University. Dosimeters were held in a WILMAD EPR sample tube Q-5M-6M-0-200m-FB (inner diameter 5mm, flat bottom). Spectrometer settings were optimized for lithium formate by Gustafsson (2008) and are presented in **Table 3**.

Table 3 Spectrometer settings.

Microwave power	20 mW
Modulation amplitude	1.2 mT
Sweep width	0.3 mT
Sweep time	168 s
Time constant	328 ms
Number of scans per dosimeter	5

The spectrometer response varies slightly from day to day. For this reason all dosimeters of one batch must be read out on the same day. Each dosimeter was read out five times. Since the sensitivity of the spectrometer also varies during the day, one dosimeter was not read out five times in a row. Instead one spectrum for each dosimeter in the batch was acquired. When all dosimeters were read out once, the first dosimeter was read out again and the procedure was repeated. Such a procedure also minimizes the effect of directional dependence of the crystals.

3.4 DOSIMETER ORGANIZATION

After the homogeneity control, the dosimeters of one batch were divided into groups of three to six, either for calibration purposes or for dose measurements. The experiments required two batches of dosimeters; Batch 1 and Batch 2. Batch 1 (dosimeter aI-fV) was used for dose measurements at Linköping Hospital and Batch 2 (dosimeter gI-LV) at Karolinska Hospital. All dosimeters were manufactured at Linköping Hospital, where the pre-irradiation and high energy photon beam calibration was performed. The exact grouping is presented in **Table 4**. The dosimeters of Batch 1 were organized in alphabetical and numerical order, that is, the first four dosimeters were set to belong to

one group, the next four to another group and so on. When the dosimeters of Batch 2 were to be divided, consideration was paid to the mean signal of each dosimeter from the homogeneity control. Ideally all groups of dosimeters should have the same signal average and standard deviation, in order to achieve maximum calibration accuracy.

Table 4 Dosimeter organization in batches and groups specified by measurement situation, quantity to be determined and dosimeter identity.

Batch	Measurement Situation	Quantity	Group	Dosimeter Identity
1	Dose Measurement ^{192}Ir	D_M 1 cm from source axis (Lkp)	*G1*	cIII, cV, dII, dIII
		D_M 3 cm from source axis (Lkp)	*G2*	bII, bIV, cI, cII
		D_M 5 cm from source axis (Lkp)	*G3*	aII, aIII, aIV, bI
	Calibration	D_0, 6 MV photon beam, (Lkp)	*G4*	eIV, fI, fII, fV
		D_1, 6 MV photon beam, (Lkp)	*G5*	dIV, dV, eII, eIII
2	Dose Measurement ^{192}Ir	D_M 1 cm from source axis (Sthlm)	*G1*	gIV, hI, hII
		D_M 3 cm from source axis (Sthlm)	*G2*	iI, iV, jV, LII
		D_M 5 cm from source axis (Sthlm)	*G3*	gI, iII, kII, LV
	Calibration	D_0, 6 MV photon beam, (Lkp)	*G4*	gIII, gV, hV, iIII, jIV, kIV
		D_1, 4 MV photon beam, (Lkp)	*G5*	gII, iIV, jI, LIII

3.5 CALIBRATION IN HIGH ENERGY PHOTON BEAMS

The dosimeters of Batch 1, *G5,* were irradiated in a 6 MV accelerator photon beam at 5 cm depth and field size of 15x15 cm^2. The dosimeters of Batch 2, *G5*, were irradiated in a 4 MV photon beam at the same depth and field size. The same phantom was used as in the pre-irradiation (Section 3.2). An ionization chamber (NE 2571 Farmer), traceable to the primary standard dosimetry laboratory BIPM in Paris and calibrated to measure absorbed dose in water following the IAEA protocol (TRS 398), was irradiated simultaneously in the same field and at the same depth as the dosimeters (**Figure 10**). The dose to water, D_1, at the position of the lithium formate dosimeters was assumed to be the same as at the position of the ionization chamber. The dose values are presented in **Table**

5. Dose profiles were studied in order to control field homogeneity. Corrections for measuring absorbed dose to water under non-reference conditions were not performed, but judged to be negligible compared to the inhomogeneity of the field. That is, dose to a small Bragg Gray cavity at the position of the ionization chamber in the PMMA phantom and a field size of 15 x 15 cm^2 was assumed to be the same as dose to water in water and a field size of 10 x 10 cm^2, which are the reference conditions. The conversion from dose to water to dose to lithium formate is described in Section 3.7.2.

The dosimeters of *G4* are not further irradiated. The signal l_w^0 from these dosimeters will determine the lower point of the calibration curve.

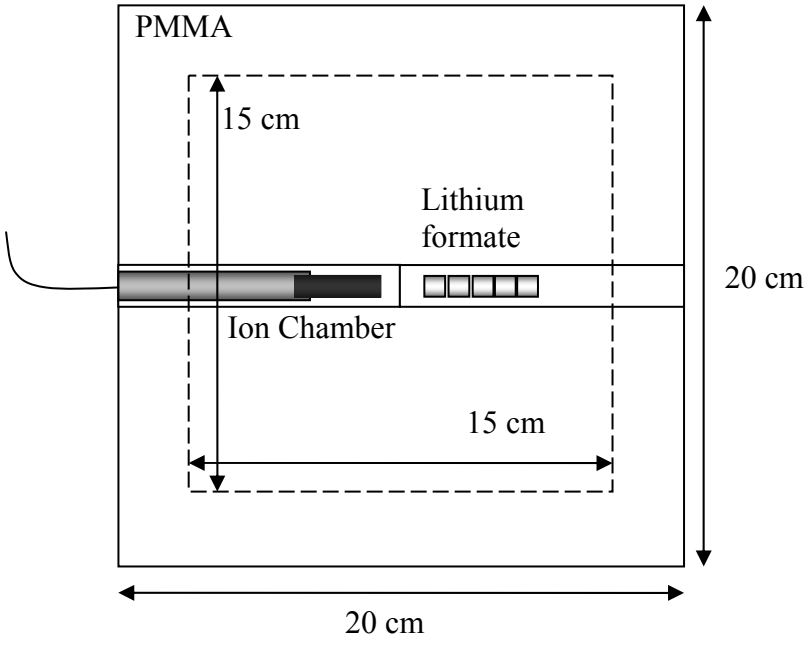

Figure 9 Calibration set-up viewed from above indicating the position of the ionization chamber and lithium formate dosimeters in the PMMA phantom. The inner square indicates the field-size. Not to scale.

Table 5 Calibration beam quality in terms of tissue phantom ratio (TPR), and dose to water at the calibration depth.

	$TPR_{20,10}$	D_1 (Gy)
Batch 1 (6 MV)	0.666	28.8
Batch 2 (4 MV)	0.622	29.9

3.6 ^{192}Ir DOSE MEASUREMENTS

Since the fading characteristics of lithium formate are not properly investigated yet, it was important that the dosimeter irradiation by ^{192}Ir and by high energy photons for calibration was performed in temporal proximity. Both irradiations of Batch 1 were carried out on the same day, while there was a separation of approximately 48 h between the ^{192}Ir irradiation at Karolinska Hospital and the calibration in Linköping of Batch 2.

The irradiation was performed in a PMMA phantom using the afterloading technique. The source used in Linköping (Batch 1) is of model Gamma Med Plus HDR (Mallinckrodt Medical B.V.) while source model Microselectron-HDR Classic (Mallinckrodt Medical B.V.) was used at Karolinska (Batch 2). The two sources are cylindrical in shape, with similar dimensions presented in **Table 6**.

Table 6 Source dimensions of the two different types used for the measurements.

	Capsule		**Source pellet**	
Source type	Diameter (mm)	Length (mm)	Diameter (mm)	Length (mm)
Gamma Med Plus HDR	0.9	4.52	0.6	3.5
Microselectron-HDR Classic	1.10	5.00	0.6	3.5

The PMMA phantom consists of 8 quadratic slabs measuring 18.1 cm when piled on each other (**Figure 11**). The sides of the slabs are 20 cm. The heights of the slabs measured separately are tabulated in Appendix (**Table 13**). Holes of 1mm height and 4.5 mm diameter were drilled in slab no 4, and of 5 mm height and the same diameter in slab no 5. The dosimeters fit into the holes with practically no air gap. The holes were drilled at the distances 1, 3 and 5 cm from the slab centre according to **Figure 12**. These distances will be referred to as the source-to-detector distances (SDD). A hole of 3 mm diameter penetrating all slabs was drilled through their centre, for the source to pass through. Full scatter conditions of at least 5 cm phantom material surrounding the dosimeters in all positions were ensured. The PMMA phantom was ordered and produced at Linköping Hospital before the study started. That is the reason why the orientation of the holes is not optimal for BT dose measurements, as the dosimeters at 5 cm lie along the same straight

line from the central hole as the dosimeters at 1 cm, so that the inner dosimeters will shield the outer from the source. The holes of 1 mm height were used to evaluate measurements with smaller dosimeters than the standard size used in a previous work (see Section 3.1).

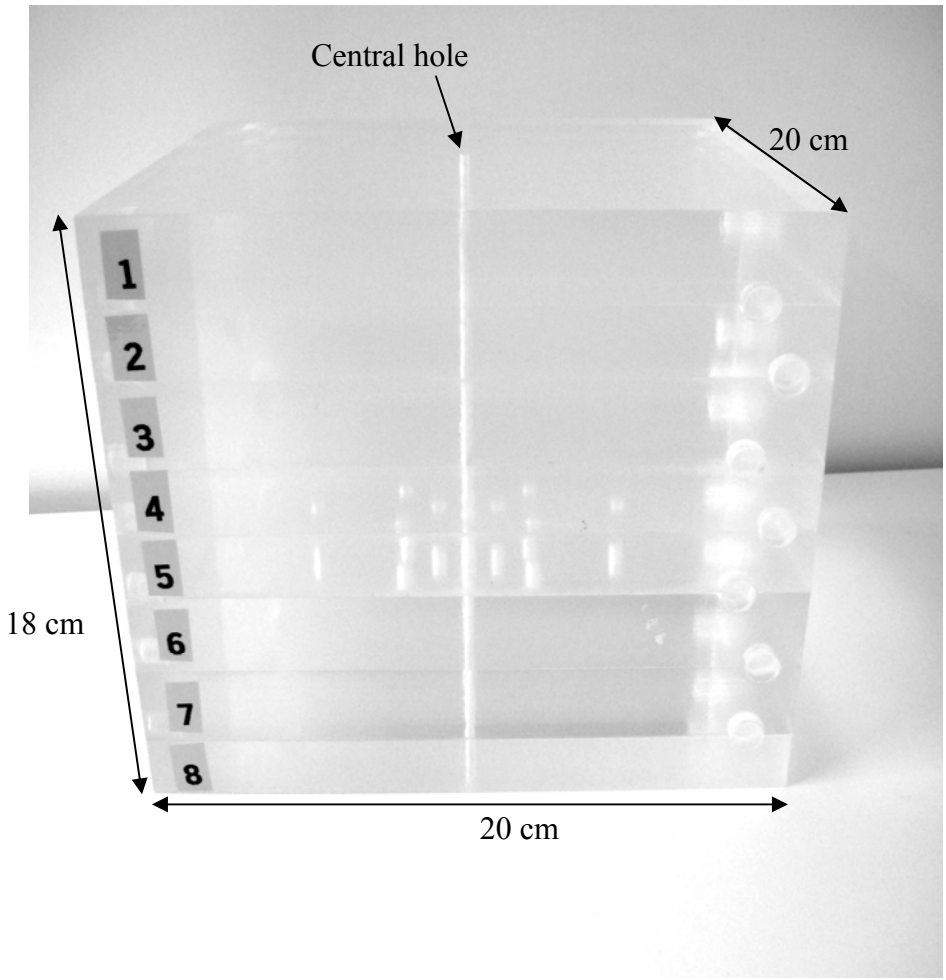

Figure 10 The PMMA phantom for dose measurements around ^{192}Ir brachytherapy source.

Since the dosimeters of 5 mm height were manufactured in standard size, they were quite large for measurements in the steep radial dose gradients around a single source. The dose falls off like $1/r^2$ around a ^{192}Ir point source, but like $1/r$ around an infinitely long line source. To minimize volume averaging in the radial direction, it was decided that the source should be stepped through many positions along the central hole, which is an approximation of the case of an infinitely long line source. As a positive side effect the

axial isodose lines became rather elliptic than round, which minimized volume averaging in axial direction too, especially at 3 and 5 cm radial distance from the source.

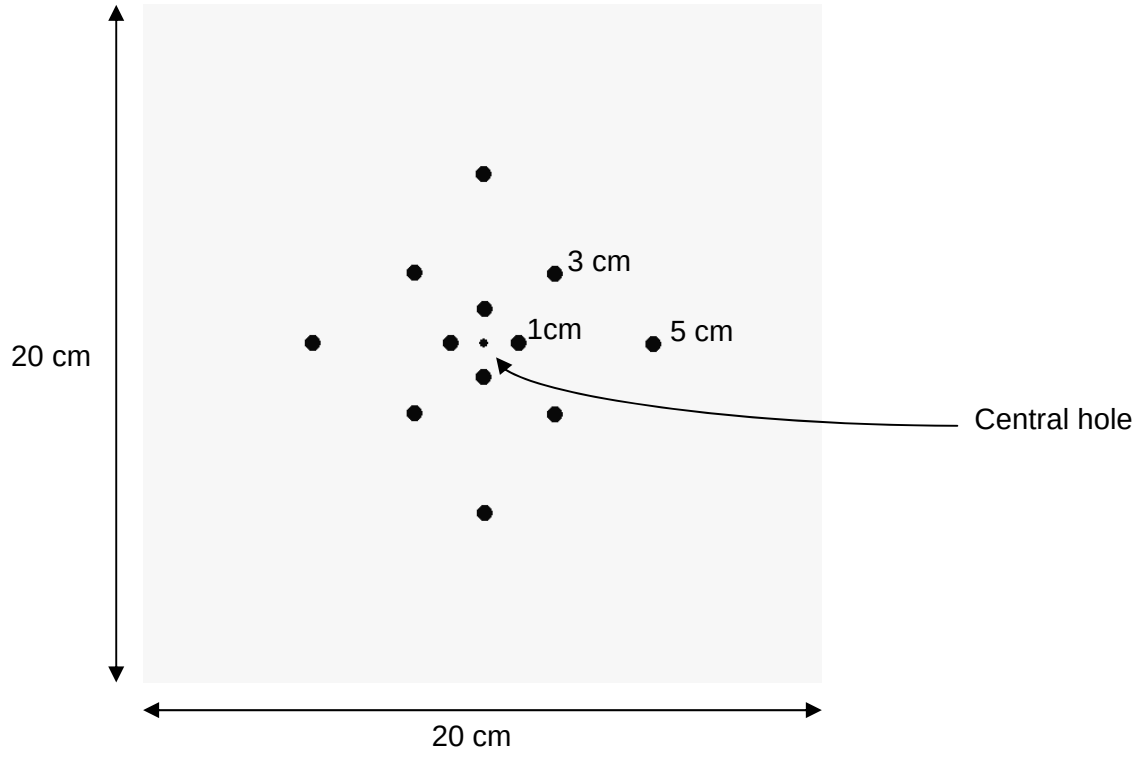

Figure 11 The positions of the dosimeters at a SDD of 1, 3 and 5 cm in slab no. 3 and 5 of the phantom.

On the day of irradiation a catheter was placed in the central hole and connected to the afterloading system. Source positions and dwell times (see **Table 14**, Appendix) in the catheter were pre-determined by the optimization method of TPS Brachy Vision (Varian Medical Systems, Software version: Eclipse BT planning 7.5.51 at Linköping Hospital) and Plato (Nucletron at Karolinska Hospital), both following the TG-43 formalism. In the measurements of Batch 1 the first source position was 5 cm above the catheter bottom according to **Figure 13** but at the catheter bottom in the measurements of Batch 2. To ensure full scatter conditions in the irradiation of Batch 2, blocks of PMMA were placed under the phantom (**Figure 14**). The last source position of both measurements was set to approximately 5 cm from the phantom top. The phantom was placed on a wooden table (Batch 1) and on a plastic container (Batch 2) (**Figure 14**). The measurement plane is at z = 8.55 cm above the catheter bottom. The point of measurement, P, is defined as the centre of the dosimeters (see also Section 3.7.2).

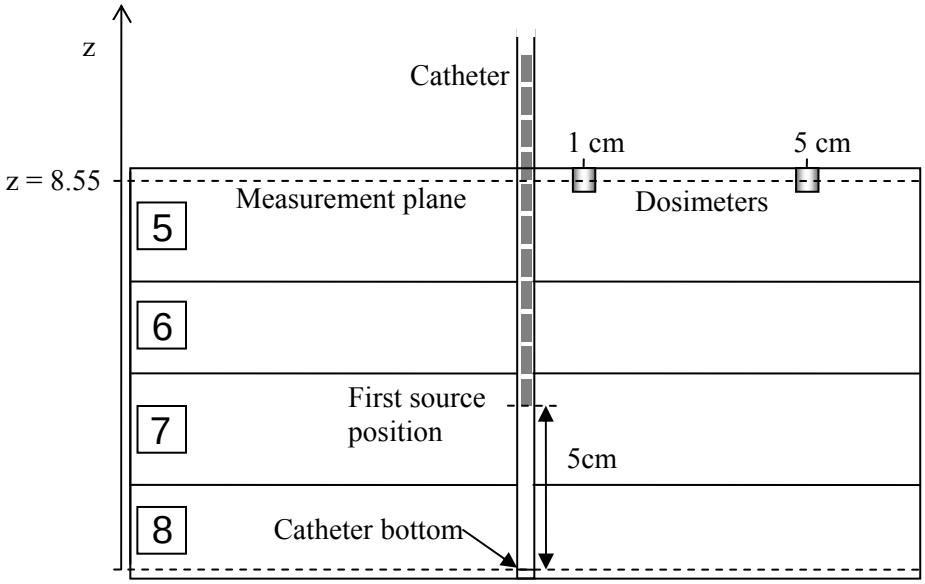

Figure 12 The experimental set-up of the dose measurement around ^{192}Ir brachytherapy source with the dosimeters of Batch 1 at Linköping Hospital. Not to scale.

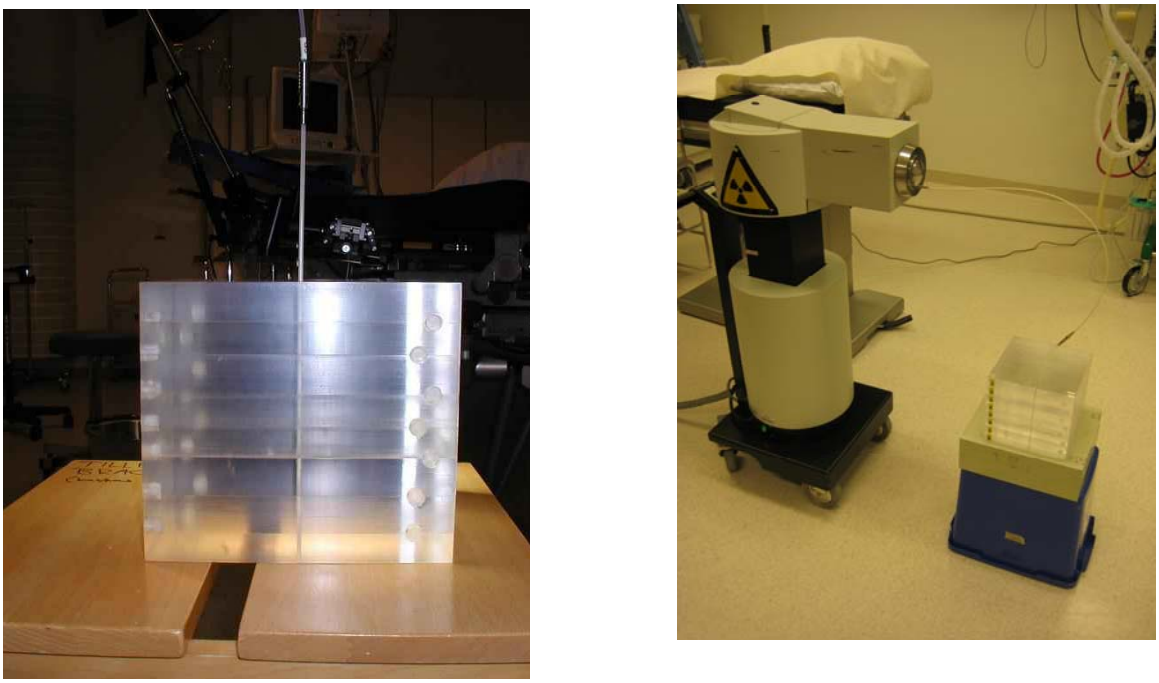

a) b)

Figure 13 Set-up of the dose measurement around ^{192}Ir brachytherapy source with the dosimeters of Batch 1 at Linköping Hospital (a) and Batch 2 at Karolinska Hospital (b).

3.7 DATA ANALYSIS

3.7.1 Calibration curve determination

The calibration curve is determined by linear regression using the weighted least-square matrix method (Thomas, Tellgren and Almlöf 1975). Since the uncertainty in dose is not negligible compared to the uncertainty in EPR signal, it must be included at an early stage using the effective variance method (Orear 1982). This method is exact in the special case of a straight line and will first be briefly described in general, before it is applied on the parameters of EPR dose measurement.

A straight line is to be fitted to a set of n measurement points (x_i, y_i). The line is described by the function $f(x) = a\ x + b$ where a is the slope of the curve and b is its intercept with the y-axis. In standard least square estimates of this function the weighted sum of the squared deviations S is minimized.

$$S = \sum_{i=1}^{n} \left(\frac{y_i - f(x_i)}{u(y_i)} \right)^2 \qquad (3)$$

$u(y_i)$ is the uncertainty in y_i. When the uncertainty in x, $u(x)$, cannot be neglected, an equivalent error in y, $u_{equiv}(y)$, is added to the uncertainty in y.

$$u_i = \sqrt{\left(u_{equiv}(y_i)\right)^2 + \left(u(y_i)\right)^2}$$

$$u_{equiv}(y) = \frac{\partial f}{\partial x} u(x) = a\, u(x)$$

u_i substitutes $u(y_i)$ in the sum of the squared deviations (Equation 3). This replacement is performed after a first estimation of the slope of the curve, a, using the standard least square method with an uncertainty in y only.

In the case of measuring signal as a function of dose described by $f(D) = a\ D + b$ the straight line is to be fitted to the measurement points (D_i, l_{wi}) with uncertainties $u(D)$ and $u(l_w)$, which is the standard deviation of the N read-outs of dosimeter i. The weighted sum of the squared deviations is thus given by

$$S = \sum_{i=1}^{n} \left(\frac{l_{wi} - f(D_i)}{u_i} \right)^2 \qquad (4)$$

where $u_i = \sqrt{\left(u_{equiv}(l_{w,i})\right)^2 + \left(u(l_{w,i})\right)^2}$ and $u_{equiv}(l_w) = a\,u(D)$.

This method might seem to be unnecessarily complicated to use, as a straight line is simply determined by the two points $(D_0, \overline{l}_w^0)$ and $(D_1, \overline{l}_w^1)$, but the main purpose of the method is to obtain the resulting variance and covariance of *a* and *b* needed for the uncertainty analysis (see Section 3.7.3). *b* will substitute $\overline{l}_w^0$ in equation 2

$$D_M = (l_w - b)\frac{1}{a}\prod_j k_j \qquad (5)$$

3.7.2 Relative energy response correction, *E(r)*

The correction term in equation 2 and 5 can be referred to as the relative energy response correction, *E(r)*, previously defined in Section 2.2 as the ratio of dosimeter response per unit dose in water at the measurement point, P, in the BT source geometry $(l_w / D)_P$, to the response per unit dose in the calibration geometry, $(l_w / D)_{cal}$, (Rivard et al 2004). Equation 5 can thus be written as

$$D_M = \left(l_w - b\right)\frac{1}{a}E(r)$$

where $E(r) = \dfrac{\left(l_w / D\right)_P}{\left(l_w / D\right)_{cal}} = \prod_j k_j$

E(r), excluding corrections for volume averaging, could be estimated by free-air measurements, irradiating the dosimeters to a known dose by X-rays matching the energy spectrum of ^{192}Ir. Such measurements are difficult to perform; e.g. there is no X-ray beam quality obtainable at the Swedish secondary standard dosimetry laboratory, SSI, matching the ^{192}Ir spectrum in water at 1, 3 and 5 cm from the source. Even if a spectrum could be substituted by an effective energy, irradiation times would be unreasonably long to achieve doses high enough for sufficient read-out precision. On top of that the uncertainty of ionization chamber dosimetry is large in the BT energy range (Rivard et al 2004).

Instead of an experimental determination of the correction, it was evaluated by calculations and by a qualitative analysis. Such an evaluation does not give any information about the intrinsic energy dependence. The dosimeters were assumed to be intrinsically linear, which means that the response is a linear function of the energy imparted.

The following corrections constitute *E(r)*; conversion from dose to water to dose to the dosimeters in the calibration situation, k_1, conversion from dose to the dosimeters to dose to water in the ^{192}Ir irradiation situation, k_2, and correction for volume averaging, k_3. The effects of using PMMA instead of water as phantom material will be discussed briefly. In the same context the effects of detector-self-absorption and medium displacement are mentioned.

Dose to dosimeter conversion, k_1

The dose to water in PMMA, $D_{w,PMMA}$, at the point of the ionization chamber in the calibration situation needed to be converted to dose to lithium formate in PMMA $D_{LiFo,PMMA}$. As a first step $D_{w,PMMA}$ was converted to dose to PMMA in PMMA, $D_{PMMA,PMMA}$, by use of Bragg Gray cavity theory, since the ionization chamber is regarded as a small cavity within the phantom material (Attix, 1986).

$$D_{w,PMMA} = D_{PMMA,PMMA}\ {}_m\overline{S}_w^{PMMA}$$

As a second step $D_{PMMA,PMMA}$ was converted to $D_{LiFo,PMMA}$. Since the electron range in PMMA irradiated by 4 and 6 MV photons (1 - 10 mm) is approximately the size of the dosimeters (4.5 - 5mm), the dosimeters were regarded as medium size. Transient charged particle equilibrium (TCPE) was assumed throughout the dosimeter volume since the dosimetry material has absorption properties similar to the phantom material. In this situation Burlin cavity theory (Burlin, 1968) was applied for the conversion. The correction factor is given by

$$f_B = \frac{D_{LiFo,PMMA}}{D_{PMMA,PMMA}} = d\left({}_m\overline{S}_{PMMA}^{LiFormate}\right) + (1-d)\left(\frac{\overline{\mu}_{en}}{\rho}\right)_{PMMA}^{LiFormate} \qquad (6)$$

where $D_{LiFo,PMMA}$ is the dose to the dosimeters, $D_{PMMA,PMMA}$ is the dose to PMMA, ${}_m\overline{s}^{LiFo}_{PMMA}$ is the ratio of mass collision stopping powers for lithium formate and water, averaged over the spectrum of secondary electrons at the measurement point, $\left(\overline{\mu}_{en}/\rho\right)^{LiFo}_{PMMA}$ is the ratio of mass energy-absorption coefficients for lithium formate and water, averaged over the photon spectrum, and d is a parameter related to the cavity size. It is given by the following equations

$$d = \frac{1 - e^{-\beta g}}{\beta g}$$

$$g = \frac{4V}{S}$$

$$\beta = \frac{16.0}{(E_{\max} - 0.030)^{1.40}}$$

where g is the mean chord length, V is the dosimeter volume, S the dosimeter surface area, β is the effective attenuation coefficient for electrons in the cavity material and E_{max} is the maximum electron energy.

For simplicity E_{max} was set to correspond to the accelerator voltage (4 and 6 MeV respectively), since small changes in E_{max} give negligible changes in k_1. (μ_{en}/ρ) was weighted over the photon energy spectrum in air produced by 4 and 6 MV accelerators (Mohan et al, 1985), where the photon energy fluence is used as weighting factor. ${}_ms_{coll}$ was weighted over the corresponding electron energy spectrum with electron fluence as weighting factor. The photon fluence of the spectrum was multiplied by the Compton cross-section of PMMA to obtain the electron fluence (XCOM, Berger et al 2005), since Compton is the dominating interaction process in the energy interval. The fact, that photons in a discrete energy interval produce electrons of a range of energies, was assumed to have minimal effect on k_1, since the stopping power ratio is extremely stable over the energy range in question. Instead the average Compton electron energy was used for values of ${}_ms_{coll}$.

The single crystals of lithium formate are quite large (< 500 μm) before being pressed to dosimeters together with paraffin, and it might questioned whether they can be regarded as homogenously mixed with the binder. An alternative approach is to regard the dosimeters as being composed of lithium formate only, which is the active material, while paraffin has no dosimetric function. The final value of f_B was thus set to be the average of the factor calculated for *pure* lithium formate and the factor calculated for a *mixture* between lithium formate and paraffin. Mass energy absorption coefficients were obtained by adding the coefficients of the atomic constituents by Bragg's additivity law. Values were obtained from the National Institute of Standards and Technology (NIST) (Hubbell and Seltzer 2004).

Mass collision Stopping Powers were obtained by use of the ESTAR program at NIST (Berger et al 2005).

The total correction factor, k_1 , is given by

$$k_1 = {}_m\overline{s}_w^{PMMA} f_B$$

The correction factor was extracted before the linear regression and included directly into equation 5.

Dose to water conversion, k_2

The dose to the dosimeters irradiated by ^{192}Ir needed to be converted to dose to water. The range of the electrons (0.05 mm) is much shorter than in the calibration situation. The dosimeters were therefore regarded as big cavities and CPE was assumed throughout the whole volume. The second correction term was given by the ratio of the mass energy absorption coefficients weighted over the photon energy spectrum of ^{192}Ir with the energy fluence, $\psi(h\nu)$, as weighting factor according to the following equation (Burlin, 1968)

$$k_2 = \frac{D_{Water}}{D_{LiFormate}} = \frac{\sum_i \psi(h\nu_i)\left(\frac{\mu_{en}(h\nu_i)}{\rho}\right)_{Water}}{\sum_i \psi(h\nu_i)\left(\frac{\mu_{en}(h\nu_i)}{\rho}\right)_{LiFormate}}$$

Values of (μ_{en}/ρ) were only obtainable for specific energies at the NIST database (Hubbell and Seltzer, 2004). Therefore logarithmic interpolation to the energies in the spectrum of ^{192}Ir in water at 1, 3 and 5 cm radial distance from the source axis was performed by Carlsson-Tedgren (personal communication). The spectra at 1 and 5 cm were derived by EGS4 MC simulations in conjunction with calculations around a mHDR-classic ^{192}Ir source (Carlsson Tedgren personal communication). The spectrum at 3 cm was obtained by linear interpolation between the spectra at 1 and 5 cm. The resulting correction factor, k_2, was set to be the average of the factor calculated for pure lithium formate and the factor calculated for a mixture between lithium formate and paraffin.

Volume averaging, k_3

The dose at the central point of the dosimeter, P, differs from the average dose to the whole dosimeter, which the EPR signal corresponds to. The reason for this so called volume averaging is that the dose does not vary linearly with distance from the source.

In radial direction e.g. the dose decreases like an average between 1/r and $1/r^2$ (see Section 3.6). The measured dose must be corrected for the deviation, if it is to be compared to the dose in one point. The orientation of the dosimeters relative to the source axis is presented in **Figure 15**.

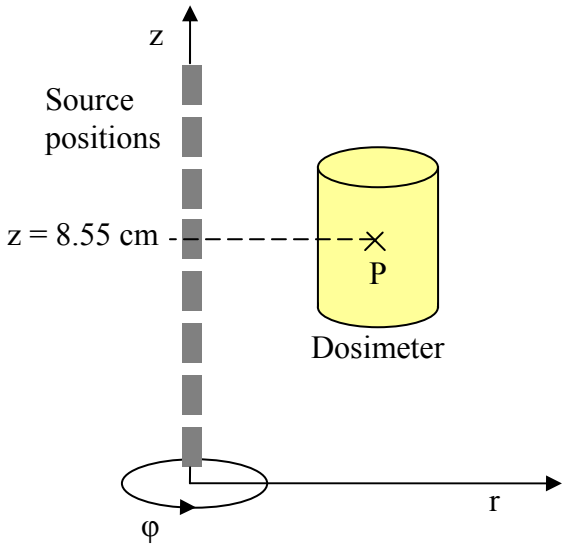

Figure 14 Dosimeter orientation relative to the source axis. Not to scale.

Brahme (1981) has proposed an easy correction method to calculate an effective point of measurement in order to account for volume averaging. The benefit of this method is that it is based on actually measured doses at several points along the direction of measurement, so that no information about the dose distribution is needed beforehand. The method can be used if the response function is constant over the dosimeter thickness in the direction of measurement. In this work it is the radial direction and the dosimeter thickness is denoted t_r. The pre-produced phantom was designed so that the dosimeter thickness in φ - direction, t_φ, varies with r (**Figure 16**). Thus the response function cannot be constant and another method to correct for volume averaging must be used. φ is the direction perpendicular to both r and z.

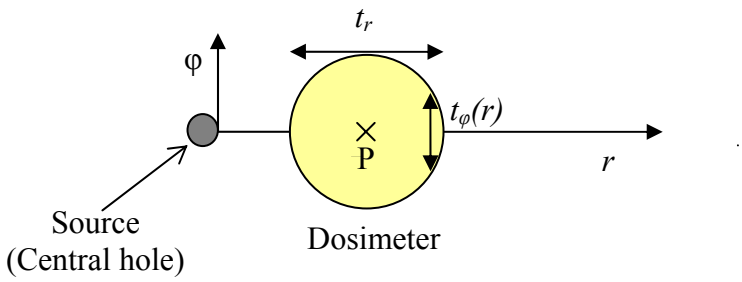

Figure 15 Dosimeter orientation in ^{192}Ir measurement geometry viewed from above. Not to scale.

The correction term was defined as the ratio between the dose to the central point of the dosimeter and the average dose to the dosimeter volume according to

$$k_3 = \frac{D_P}{D_{average}}$$

$$D_{average} = \frac{\iiint_V D(r,z,\varphi)\,dr\,dz\,d\varphi}{\iiint_V dr\,dz\,d\varphi}$$

The correction was estimated by averaging the dose from the TPS in r and z direction, while volume averaging in φ-direction was regarded as negligible. To calculate an average dose value in radial direction, $\bar{D}_r$, the depth dose curve of the measurement plane, obtained from the TPS Brachy Vision was used (see **Figure 17**). Depth dose curves were only obtainable from the TPS used at Linköping Hospital (Batch 1). The correction derived from them was also applied on the data of Batch 2.

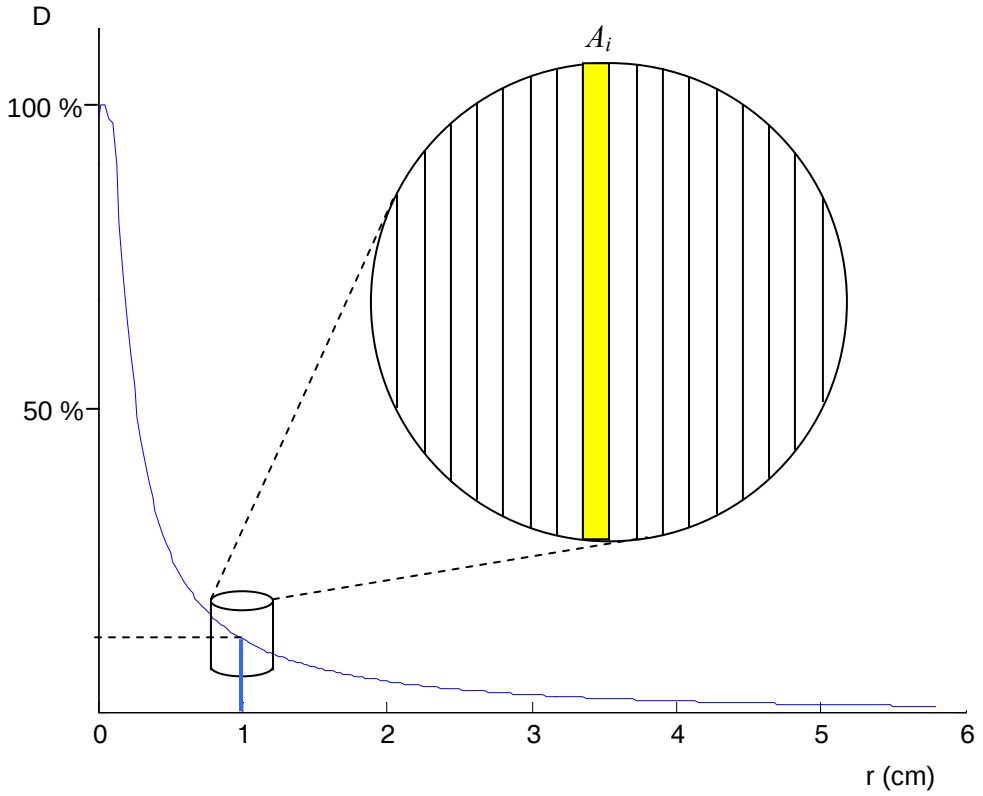

Figure 16 Depth dose curve at z = 8.55 cm. The position of the dosimeter at 1 cm is indicated as well as the compartments of its circular surface area used to determine the weighting factor for the volume averaging correction. Not to scale.

An average dose, $\bar{D}_r$, was calculated, in an interval corresponding to the dosimeter size given by $SDD - R \le r \le SDD + R$, where R is the dosimeter radius.

$$\bar{D}_r = \sum_{i=1}^{N} w_i D_i$$

The weighting factor, w_i, was obtained by dividing the circular area, A, of the dosimeters into N compartments according to **Figure 17**.

$$w_i = \frac{A_i}{A}$$

where A_i the area of compartment i given by

$$A_i = \frac{2R}{N} t_\varphi(r_i)$$

$2R/N$ is the compartment thickness and $t_\varphi(r_i)$ is the dosimeter thickness at r_i, the centre of compartment i. The number of compartments was set to $N = 18$ in order to match the data intervals of the dose profiles.

A radial dose average was calculated for 7 different positions along the z-axis (z = 82.5, 83.5, 84.5, 85.5 86.4, 87.4, 88.4). The dose from the TPS corresponding to point P was now divided by the total average of these 7 values to obtain an estimation of k_3. This was done for all three measurement points; 1, 3 and 5 cm radial distance from the source. D_i

An estimation of the size of the correction in radial direction $k_{3,r}$ was obtained from the radial average at z = 85.5. An axial correction factor, $k_{3,a}$, was obtained by an average of the dose at r = 1, 3 and 5 cm respectively in the 7 different $r\varphi$-planes.

Effects of measurement medium and phantom size on absorbed dose, k_4

According to TG-43 the energy response also depends on detector self-absorption, medium displacement, and conversion from the measurement medium to liquid water (Rivard et al 2004). A study on the choice of phantom material for dosimetry of ^{192}Ir sources supports the use of PMMA as phantom material instead of water under full scatter conditions, as it is quite water equivalent (Meli et al 1988). See Section 2.2. Compton scattering is the dominating interaction process at the energies of ^{192}Ir. The faster absorption of primary photons in PMMA, due to a higher density than water, is thus compensated for by faster build up of secondary photons. The same reasoning can be applied on the effects of detector-self absorption and medium displacement, as lithium formate also resembles water to a high degree, but has a higher density. Furthermore the dosimeters are much smaller than the distances that the photons have to travel in the

PMMA, why deviations from the model should have little effect on the dose to the dosimeters. A correction factor accounting for detector self-absorption, medium displacement, and conversion from the measurement medium to liquid water is set to unity.

The PMMA phantom used in this work is smaller than the reference water phantom on which the TPS dose data is based. This leads to a lower dose to water in the small phantom relative to the large phantom at 3 and especially at 5 cm, due to the lower contribution by scattered radiation. Carlsson Tedgren (personal communication) has performed Monte Carlo calculations of the dose to water, $\left(D_w(20,40)\right)_{PMMA}$, from ^{192}Ir BT source at different depths in a PMMA cylinder of 20 cm height and 10 cm radius, which is comparable to the phantom used in this work. The result was compared to dose calculations for a water cylinder of 40 cm height and 20 cm radius, which is comparable to the TPS reference phantom. The correction factor for phantom size is given by the ratio of the dose for the two phantom sizes and materials.

$$k_4 = \frac{\left(D_w(10,20)\right)_{water}}{\left(D_w(20,40)\right)_{PMMA}}$$

where $\left(D_w(10,20)\right)_{water}$ is the dose to water in the large water phantom. This correction factor is not included in the relative energy response correction as it is highly independent of the dosimeter material and shape.

3.7.3 Uncertainty analysis

Three main components contribute to the uncertainty in measured dose; uncertainty given by the dose equation (Equation 5), uncertainties in dose delivery to the dosimeters in the ^{192}Ir irradiation situation and in reproducibility of measurements. The contributing components are listed in **Table 7**.

Table 7 List of uncertainty components, notation and type.

Component	Notation	Type
Dose equation:		
EPR signal corresponding to measured dose	$u(l_w)$	A
Calibration:		
Slope of the curve	$u(a)$	A+B
Curve intercept with signal axis	$u(b)$	A+B
Covariance of a and b	$u(a, b)$	A+B
Correction factors:		
Dose to dosimeter conversion factor	$u(k_1)$	B
Dose to medium conversion factor	$u(k_2)$	B
Volume averaging correction factor	$u(k_3)$	B
Phantom material substituting water	$u(k_4)$	A+B
^{192}Ir dose delivery system:		
Source positioning in radial direction	$u(D)$	B
Source positioning in axial direction	$_{pos,r}$	B
Source calibration	$u(D)_{pos,z}$ $u(D)_{cal}$	A+B

Uncertainty given by the dose equation.

The total combined uncertainty in measured dose obtained by the dose equation (5), $u(D_M)$, was estimated by adding the uncertainties of its parameters according to the law of propagation (ISO 1995).

$$u^2(D_M) = \left(\frac{\partial D}{\partial l_w}u(l_w)\right)^2 + \left(\frac{\partial D}{\partial a}u(a)\right)^2 + \left(\frac{\partial D}{\partial b}u(b)\right)^2 + 2\frac{\partial D}{\partial a}\frac{\partial D}{\partial b}u(a,b) + \sum_j \left(\frac{\partial D}{\partial k_j}u(k_j)\right)^2$$

The uncertainty in l_w, $u(l_w)$, is given by the standard deviation of the signal mean from the different read-outs of one dosimeter and by the uncertainty due to the inhomogeneous

dose response of the dosimeters given by the relative standard deviation of the batch signal (1%) obtained by the homogeneity control .

$$u(l_w) = \frac{\sigma_{l_w}}{\sqrt{n}} + 0.01\, l_w$$

The uncertainty of the parameters of the calibration curve, *a* and *b*, is given by the covariance matrix obtained by linear regression. It depends on the uncertainties of the input parameters D_0 and D_1 and their corresponding signals. See Section 2.4. The relative uncertainty in calibration dose, $u(D_1)/D_1$, is the relative uncertainty in the calibration factor, $u(N_{D,w})/ N_{D,w}$, (± 0.5 %, k = 1) added to the relative uncertainty due to field homogeneity imperfection, $(u(D_1)/D_1)_{field}$. The latter was determined by assuming a normal distribution around the value D_1, obtained by the ionization chamber measurement, and by estimating a probability of 0.5 that the dose at the position of the dosimeters lay in the interval $D_1 \pm 0.0025\, D_1$. According to the Guide to the expression of uncertainties in measurement (GUM) the uncertainty can then be set to 1.48 of half that interval (ISO 1995). The relative uncertainty in dose due to field homogeneity imperfection is thus 0.37%. The addition is performed as follows

$$\left(u(D_1)/D_1\right)^2 = \left(u(N_{D,w})/N_{D,w}\right)^2 + \left(u(D_1)/D_1\right)^2_{field}$$

The uncertainty in D_0 is assumed to be the relative uncertainty in D_1 multiplied by the pre-irradiation dose, D_0'.

The uncertainty in correction factor k_1 was estimated by analyzing how several different parameters affected the size of it. The parameters causing the largest change in the Burlin equation (6) are E_{max} and *d*. It can be discussed whether the lithium formate crystals are homogenously mixed with the paraffin or if they should be regarded as small cavities within the binding material. The value of k_1 is somewhat lower calculated for pure lithium formate than for a mixture of the two materials. These three parameters are combined to give the highest and lowest possible value of k_1 within reasonable limits. These limits are generously set and presented in **Table 8**. It can also be discussed whether the dosimeters are to be regarded as medium size cavities, which is assumed in this work.

The uncertainty due to this assumption was estimated by comparing the size of the mass collision stopping power ratio, ${}_m\bar{s}^{LiFo}_{PMMA}$, and the mass energy absorption coefficient ratio $\left(\bar{\mu}_{en}/\rho\right)^{LiFo}_{PMMA}$ with the resulting correction factor k_1. The uncertainty due to the assumption of an equal photon energy spectrum in air and in PMMA at 5 cm depth is regarded as negligible, since small differences affect the absorption ratios very little. The uncertainties in stopping powers and absorption coefficients are assumed to cancel in the ratios between different materials. The uncertainty due to incomplete CPE is regarded as negligible compared to the other factors contributing to the uncertainty in k_1.

Table 8 Maxiumum and minimum limits of the parameters giving maximum and minimum correction factor k_1.

Composition	E_{max}	h	d	k_1
100% lithium formate	Max: 6 and 4 MeV resp.	Min: 4.5 mm	Max	Min
90% lithium formate 10% Paraffin	Min: 5 resp. 3 MeV	Max: 5.5 mm	Min	Max

The uncertainty in correction factor $u(k_2)$ is estimated in a similar way, with the exception that there is no factor d to vary. The uncertainty is thus only based on the uncertainty due to the composition of the dosimeters and the uncertainty in which cavity theory should be applied.

The maximum and minimum values of k_x (x = 1, 2), $k_x^{\max}$ and $k_x^{\min}$ respectively, were used for an estimation of a numerical value of $u(k_x)$. The calculation was divided in two different cases; the uncertainty due to the composition of the dosimeters and the variables of the Burlin equation, $u_A(k_x)$, and the uncertainty in applied cavity theory, $u_B(k_x)$.

A triangular distribution between $k_x^{\max}$ and $k_x^{\min}$ was assumed with a probability of 100% that the true value lay in the interval. According to GUM the uncertainty in k_x for the different cases i, is then given by:

$$u_i(k_x) = \frac{k_x^{\max} - k_x^{\min}}{2\sqrt{6}}, \quad x = 1, 2, \quad i = A, B$$

(ISO 1995)

The total combined uncertainty of k_x was calculated as follows:

$$u(k_x) = \sqrt{\left(u_A(k_x)\right)^2 + \left(u_B(k_x)\right)^2}$$

The uncertainty in the volume averaging factor was estimated by studying what effect the uncertainty in positioning has on the factor.

The uncertainty in the correction factor for phantom size, $u(k_4)$, is estimated to be 0.5 % (Carlsson Tedgren personal communication).

Uncertainty in dose delivery.

The uncertainty in source positioning in axial direction of ± 1 mm (k = 2) is stated by the vendor and is used to determine the corresponding uncertainty in dose, $u(D)_{pos,z}$. A numerical value is set to be equal the change in TPS dose with a change in position corresponding to ± 1 mm, at 1, 3 and 5 cm radial distance from the source central axis according to Figure 18, 19 and 20.

The uncertainty in source positioning in radial direction is estimated to be ± 1 mm as well, and $u(D)_{pos,r}$ is estimated the same way as $u(D)_{pos,z}$. It accounts for the air gap between the catheter and the central hole of the phantom, the extent to which the source can move within the catheter and any possible unevenness of the dosimeter surface. Since no dose profiles were obtainable from the TPS used at Karolinska Hospital the same positioning uncertainty is used for both batches. The certificate for the ^{192}Ir source stated the uncertainty in source calibration to be +- 5% of the Reference Air Kerma Rate at a confidence level of 99.7%, which gives one standard uncertainty of approximately 2 %. Thus $u(D)_{cal} = 0.02\ D_M$

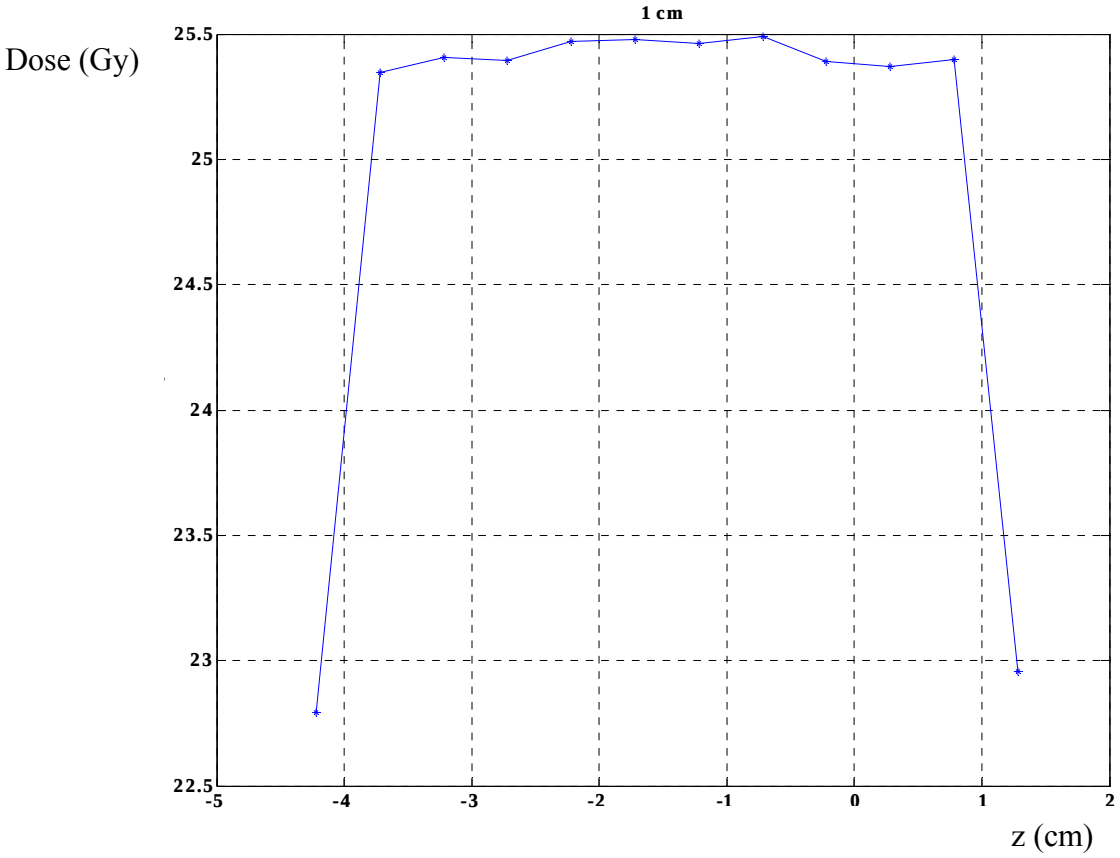

Figure 17 Dose profile at 1cm radial distance from the source from the first ^{192}Ir irradiation (Brachy Vision at Linköping Hospital)

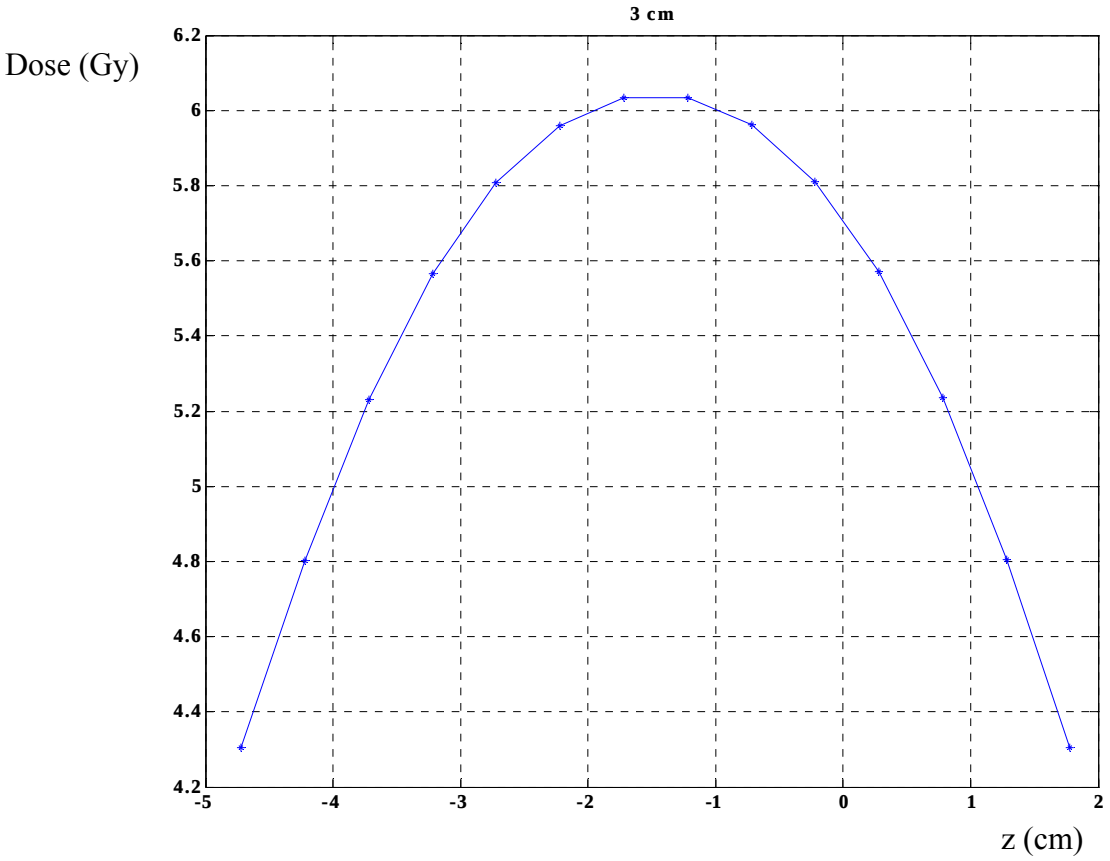

Figure 18 Dose profile at 3 cm radial distance from the source from the first ^{192}Ir irradiation (Brachy Vision at Linköping Hospital)

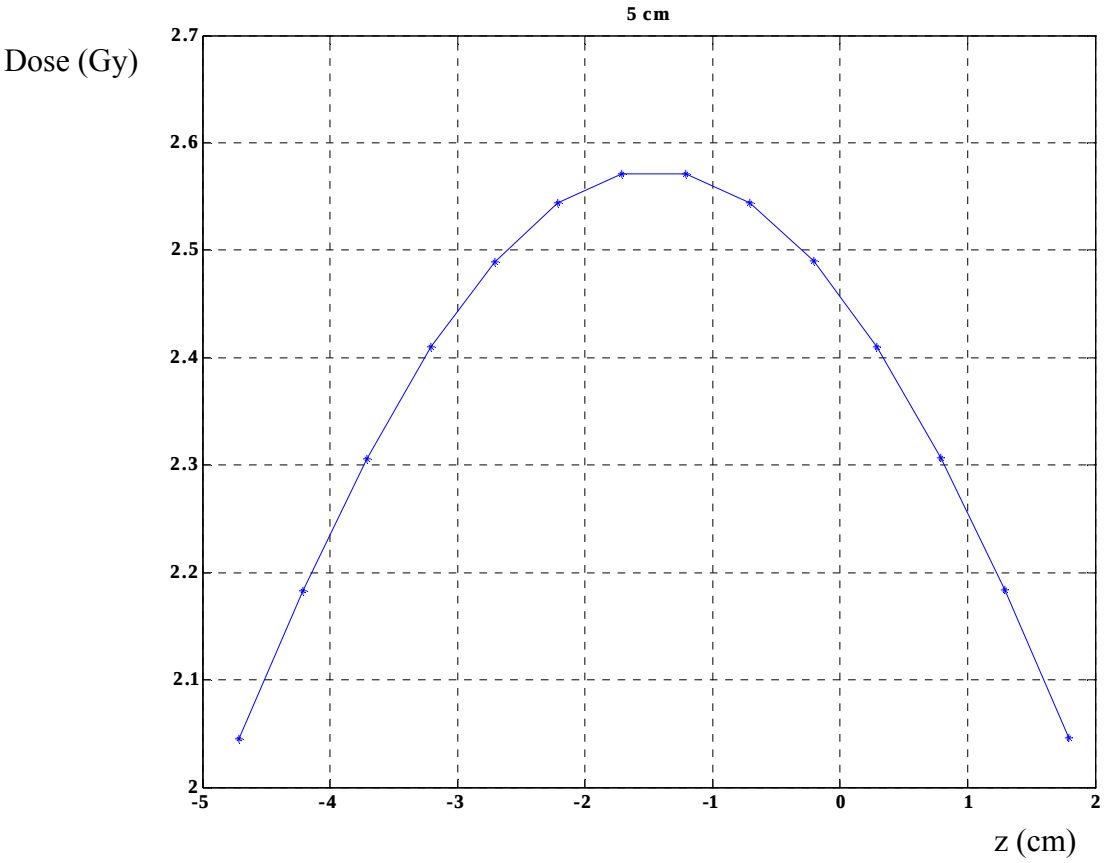

Figure 19 Dose profile at 5 cm radial distance from the source from the first ^{192}Ir irradiation (Brachy Vision at Linköping Hospital)

Total combined uncertainty.
$u(D)_{pos,z}$, $u(D)_{pos,r}$ and $u(D)_{cal}$ are added to $u(D_M)$ to obtain the total combined uncertainty

$$u(D)_{tot} = \sqrt{u^2(D_M) + u^2(D)_{pos,z} + u^2(D)_{pos,r} + u^2(D)_{cal}}$$

Four dosimeters[1] were used to establish the dose at each distance from the source. The uncertainty in the average dose, $u(\bar{D}_M)$, can be calculated according to the law of error propagation (GUM). This is of course not the same as the average uncertainty in measured dose, $\bar{u}(D_M)$. See Section 4.

[1] For measurements at 1 cm (Batch 2) only 3 dosimeters were used, while the fourth hole was plugged by a dummy dosimeter.

Uncertainty in TPS dose values

Generic values of Monte Carlo uncertainties stated by the TG 43 report (Rivard *et al* 2004) are used as an estimate of $u(D_{TPS})$. The uncertainty is 2.5 % at 1 cm radial distance from a point source and 5% at 5 cm. The average of these two values is used as uncertainty at 3 cm.

4 RESULTS

The conversion factor, k_1, is 0.924 for both the 4 and 6 MV calibrations. The conversion from dose to lithium formate to dose to water is 1.0799, 1.0818 and 1.0848 at 1, 3 and 5 cm from the source respectively. The volume averaging correction factor, k_3, is 0.9885 at 1 cm, 1.0015 at 3 cm and 1.0031 at 5 cm from the source. The correction for a measurement phantom differing from the reference phantom of the TPS, k_4, increases with distance from 1.007 at 3 cm to 1.028 at 5 cm distance from the source and is negligible at 1 cm. The correction factors k_1 - k_3 are presented in **Table 9** and **Figure 21**.

The correction for volume averaging in radial direction, $k_{3,r}$, is smaller than one at all distances from the source, with the largest deviation from unity at 1 cm form the source. The correction in axial direction, $k_{3,a}$, is larger than one at all distances, with the largest deviation at 5 cm from the source. The values are presented in **Table 10** and **Figure 22**. These tendencies can easily be realized by studying dose profiles and depth dose curves of the source stepping sequence used in this work (see Figure 17-20), since the application of a line source is less applicable at large distances from the source and dose gradients are flatter outwards.

The dose given by the TPS, D_{TPS}, is presented in **Table 11** together with the measured dose, $\bar{D}_M$, calculated as an average of the four dosimeters at each distance from the source. The average absolute uncertainty in dose, $\bar{u}(D_M)$, and the relative deviation $(\bar{D}_M - D_{TPS})/D_{TPS}$ are presented in the same table. The relative standard deviation in measured dose ($\sigma_{D_M}/\bar{D}_M$) was 0.3 - 3 %.

When comparing measured dose values with those given by the TPS for Batch 2, it was found that the TPS value at 1 cm must have been misread. For this reason the experiment was simulated by Carlsson Tedgren Å (personal communication). New values for comparison were calculated and for simplicity referred to as D_{TPS}. This was done by the MC program EGS4 and the geometry described in section 3.6 was used for input. Since the correct phantom size is used for these calculations correction factor, k_4, is not applied on the measured dose values for Batch 2.

The absolute dose values range from approximately 2.5 Gy at 5 cm from the source to 25 Gy at 1 cm from the source. The minimum and maximum relative deviation between measured dose and dose given by the TPS (or calculated dose) is 1.4 % and 3.2 % respectively.

The components contributing to the total combined uncertainty in dose, $\overline{u}(D_M)$, are presented in **Table 12**. The total combined uncertainty at coverage factor k = 1 is 5 % at 1 cm distance from the source and 3 % at 3 and 5 cm from the source.

Table 9 The values of the individual correction factors, k_1 - k_3 and the relative energy response correction $E(r)$.

SDD	k_1	k_2	k_3	$E(r) = \prod_i^3 k_i$
1 cm	0.9242	1.0799	0.9885	0.9849
3 cm	0.9242	1.0818	1.0015	0.9996
5 cm	0.9242	1.0848	1.0031	1.0039

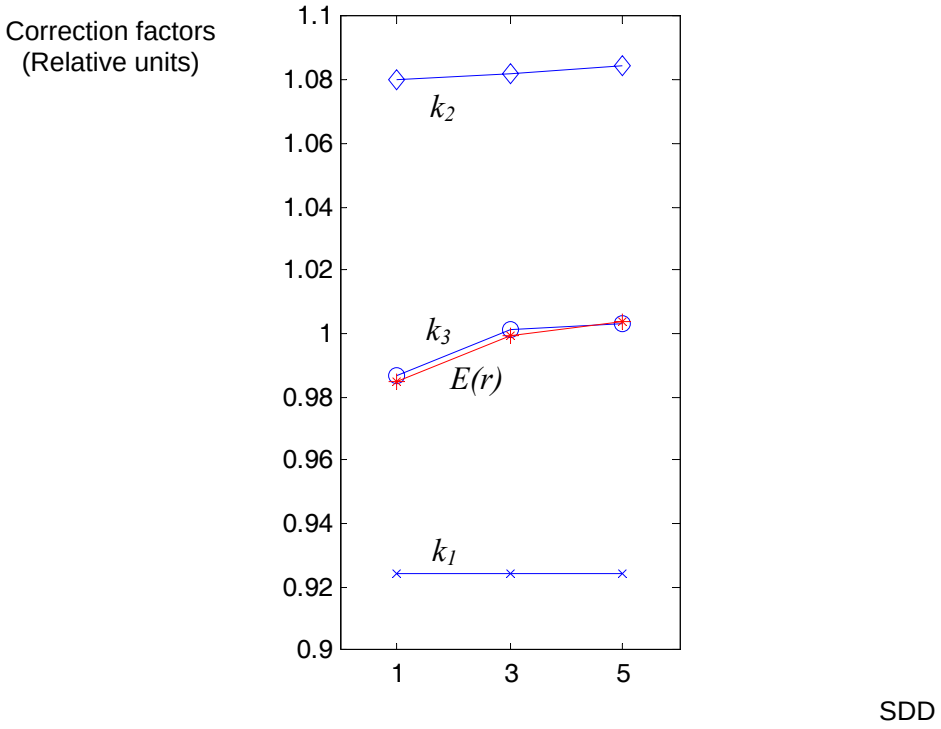

Figure 20 Correction factors k_1, k_2, k_3 and their product, the relative energy response correction, $E(r)$.

Table 10 Correction factor, k_3, obtained by averaging in radial ($k_{3,r}$) and axial ($k_{3,a}$) direction separately for Batch 1.

SDD	$k_{3,r}$	$k_{3,a}$
1 cm	0.9868	1.0021
3 cm	0.9977	1.0038
5 cm	0.9989	1.0042

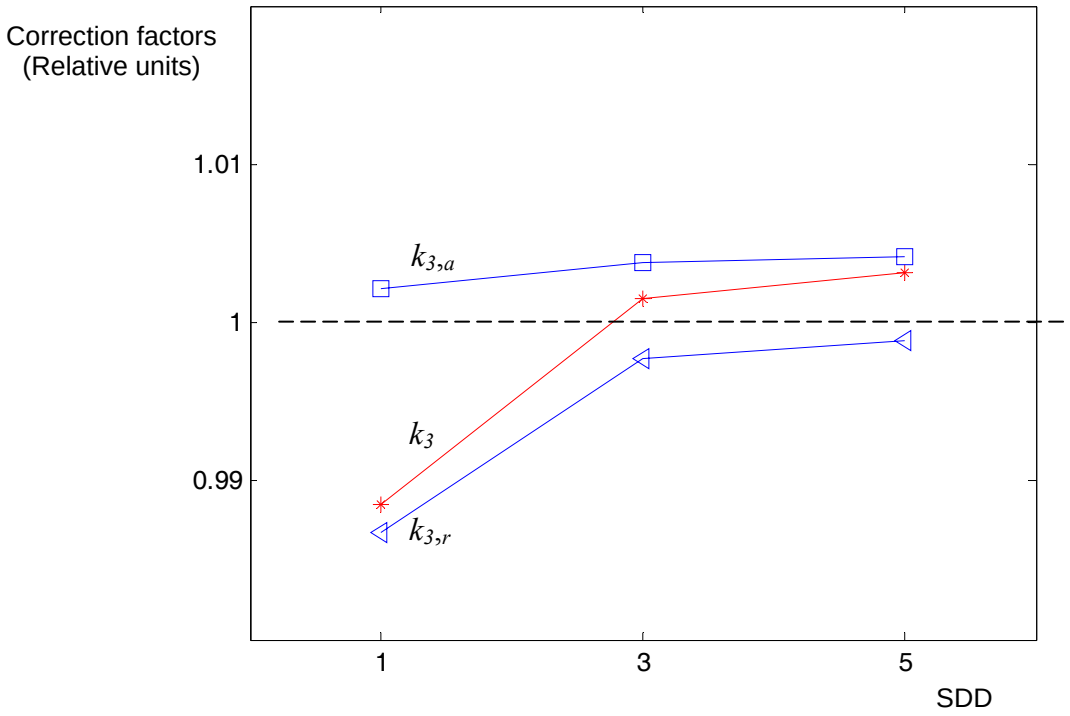

Figure 21 Volume averaging correction factor, k_3, and its components in radial and axial direction, $k_{3,r}$ and $k_{3,a}$ respectively.

Table 11 Measured dose, $\bar{D}_M$, dose given by the treatment planning system, D_{TPS}, and the relative deviation between the two values. $\bar{D}_M$ is an average of the four dosimeters measuring dose at the same distance from the source, except for the value of Batch 2 at 1cm, where only 3 dosimeters were used. Uncertainty in $\bar{D}_M$ is given at coverage factor k = 2.

Batch	SDD	D_{TPS} (Gy)	$\bar{D}_M$ (Gy)	$\frac{\bar{D}_M - D_{TPS}}{D_{TPS}}$
1	1 cm	25.4 ± 0.6	25.0 ± 2.5	-2.1 %
	3 cm	6.04 ± 0.2	5.9 ± 0.4	-1.6 %
	5 cm	2.57 ± 0.12	2.49 ± 0.15	-2.8 %
2	1 cm	25.3 ± 0.6	24.8 ± 2.5	-3.3 %
	3 cm	6.5 ± 0.2	6.7 ± 0.4	2.0 %
	5 cm	3.1 ± 0.15	3.1 ± 0.19	1.0 %

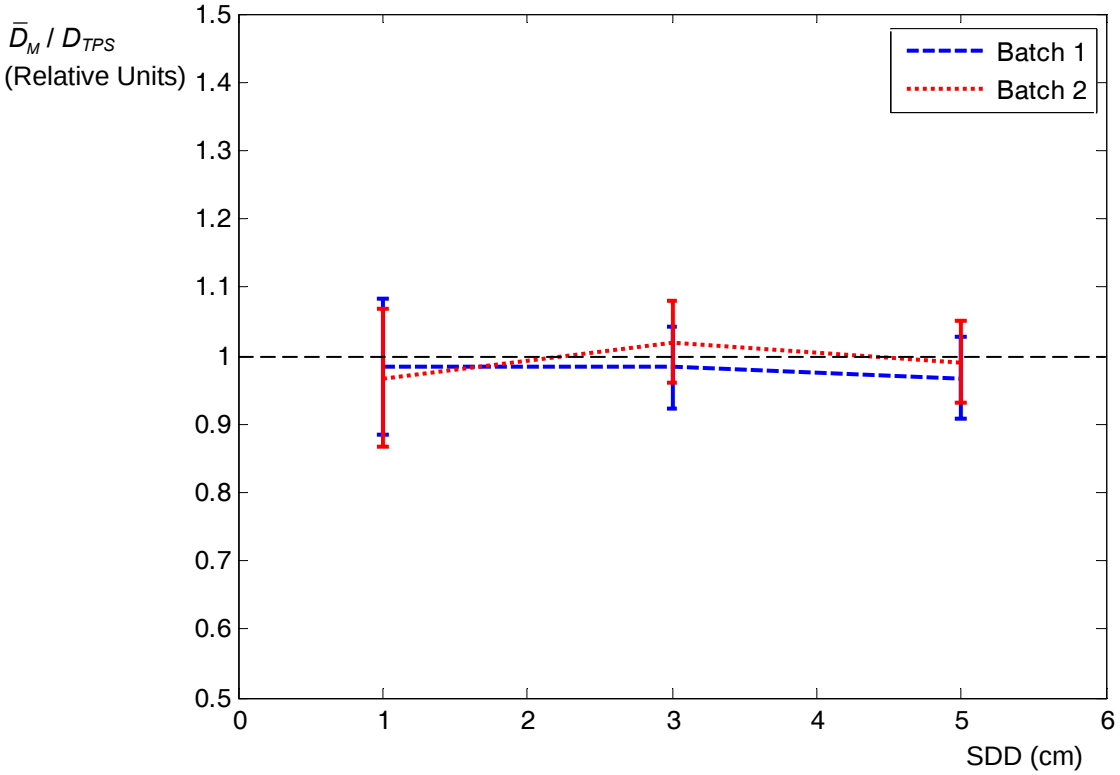

Figure 22 Ratio between measured average dose, $\bar{D}_M$, and dose given by the TPS, D_{TPS}, at the three different distances from the source for Batch 1 and Batch 2. The average uncertainty, $\bar{u}(D_M)$, at coverage factor k = 2, is indicated by the error bars.

Table 12 List of the components contributing to the average relative total combined uncertainty in D_M at coverage factor k = 1.

Component	Batch 1			Batch 2		
	1cm	3 cm	5 cm	1cm	3 cm	5 cm
Dose equation:						
Uncorrected dose ($D_M = (l_w - b)\frac{1}{a}$ **)**	1.3 %	1.8 %	2.1 %	1.5 %	1.6 %	2.1 %
Correction factors:						
Dose to dosimeter conversion factor	0.9 %	0.9 %	0.9 %	0.9 %	0.9 %	0.9 %
Dose to medium conversion factor	0.05 %	0.05 %	0.05 %	0.05 %	0.05 %	0.05 %
Volume averaging correction factor	0.14 %	0.1 %	0.1 %	0.14 %	0.1 %	0.1 %
Phantom material substituting water	0.5 %	0.5 %	0.5 %	0.5 %	0.5 %	0.5 %
^{192}Ir dose delivery system:						
Source positioning in radial direction	4 %	1.7 %	1.3 %	4 %	1.7 %	1.3 %
Source positioning in axial direction	0.1 %	0.3 %	0.3 %	0.1 %	0.3 %	0.3 %
Source calibration	2 %	2 %	2 %	2 %	2 %	2 %
Total combined uncertainty in D_M	**5 %**	**3 %**	**3 %**	**5 %**	**3 %**	**3 %**

5 DISCUSSION

The factors included in the relative energy response correction are all in the order of 0.1 to 1 % (see **Table 9** and **Figure 21**). The dose conversion factors, k_1 and k_2, tend to cancel each other. Therefore the correction for volume averaging, k_3, dominates the total energy response correction, $E(r)$.

Since k_2 is calculated by averaging over a single source spectrum it is probably underestimated, especially at 5 cm SDD. The relative contribution to the total dose from the source positions far away is higher at large SDD than at small SDD.

The measured absorbed dose agrees well with the dose given by the treatment planning system. The deviations are smaller than the calculated uncertainty (coverage factor k = 2) and range from 1.0 – 3.3 %.

The average relative 1 σ total combined uncertainty in D_M, is 3 % for the measurements at 3 and 5 cm from the source, but 5 % for the measurements at 1 cm. The component causing this large difference is the uncertainty in source positioning in radial direction (**Table 12**). This difference as well as the absolute size of the uncertainty at all three SDD would be even larger if the measurements were performed with the source in one position only, since dose gradients would be steeper. The uncertainty should be much smaller though if the dose is determined by an average of the four dosimeter positions at one SDD, since an increase in dose at one side leads to a decrease at the opposite side. The size of the uncertainty in source positioning in axial direction and in the volume averaging correction factor would also be larger in the single source case.

Interestingly the uncertainty in uncorrected dose, which is of statistical kind, is as low as 1.3 – 1.5 % for the high doses of about 25 Gy at 1 cm. If an individual sensitivity factor were applied, defined as the individual dosimeter dose response divided by the average dose response of the batch, this uncertainty could possibly be further reduced. The dose response stability of lithium formate detectors must be investigated before such an application can be performed.

As mentioned above the dose to water conversion factor, k_2, is probably underestimated. This has not been accounted for in the uncertainty analysis.

It can be questioned whether it is relevant to compare the measured doses to values of the TPS. Since ionization chamber measurements have large uncertainties at BT energies, TPS was regarded as the most reliable source for comparison, as uncertainties in dose delivery are accounted for.

The size of the total combined 1 σ uncertainty in dose (3-5 %) is comparable to the uncertainty in dose rate of 7-9 % for the LiF TLD single source dosimetry system stated by TG-43. Of course some uncertainty components are larger for the latter case, since dose gradients are steeper around a single source, and a fair comparison between the systems can only be performed if experiments are equivalent.

An obvious advantage of the lithium formate dosimetry system compared to LiF TLD is the larger dynamic range in absorbed dose. The LiF dosimeter has an upper dose limit of approximately 1 Gy before supralinearity becomes a source of uncertainty. Since the transit dose from sources of clinically relevant HDR ^{192}Ir sources may be significant but not properly corrected for by most TPS, it could give a high contribution to the total dose to LiF dosimeters according to several authors (Guzman Calcina *et al* 2005, Wong *et al* 2001, Bastin *et al* 1993 and Houdek *et al* 1992). Therefore, measurements using LiF dosimeters are often performed after the source has decayed to levels below those used clinically, so as to limit the transit dose to contribute a small fraction to the total absorbed dose. Using the lithium formate dosimetry system, this problem can be avoided simply by giving high enough doses for the transit dose to become negligible and measurements can be made using sources with clinically relevant activities.

A possible drawback of the study might be that some important dosimetric properties of lithium formate, such as dose rate dependence, fading characteristics intrinsic energy response and dose response stability should have been examined separately, before an application study such as this was performed. The dose rate of single accelerator pulses is much higher than the dose rate of radioactive sources. In recent studies the response of lithium formate irradiated by accelerator photon beams of 6-20 MV has been compared to the response to ^{60}Co irradiation (Malinen et al 2007, and Vestad et al 2003). The results were analyzed in terms of energy dependence, and showed a smaller energy response for lithium formate than for LiF. The results can also be used as an indication that the high accelerator dose rate does not essentially affect the response compared to radioactive sources. This study should be regarded as a feasibility study, and the results show that it is well worth spending time on investigating the mentioned dosimetric properties.

6 CONCLUSIONS AND OUTLOOK

Lithium formate EPR has been shown to have a large potential for dosimetry in the energy range of BT source ^{192}Ir.

If the dosimeters are given high enough doses (preferably > 20 Gy), the precision of the dosimetry system should be comparable to LiF TLD. The precision of the latter system cannot be enhanced by increasing doses, since its supralinearity above a certain dose level reduces precision.

Due to the low energy dependence of lithium formate it is especially promising for use in situations where the energy spectrum is unknown. A possible field of application could be the verification of multi source treatment plans in BT.

Before the dosimetry system can be used for experimental verification of the dose distribution around single sources or other situations where dose gradients are steeper than in the present work, methods to produce smaller and less fragile dosimeters must be developed, since positional accuracy and low volume averaging are crucial for accurate dose determinations.

A comparative study between lithium formate EPR and LiF TLD, with experiments of equal set-up for both materials should give better information about the suitability of lithium formate for experimental determination of the dose distribution around BT sources.

7 ACKNOWLEDGEMENTS

This study was initiated by Håkan Gustafsson, Åsa Carlsson Tedgren and Eva Lund. Åsa Carlsson Tedgren was my supervisor and helped me steering the project in the right direction. I am very grateful for her kind supportiveness and accessibility. Special thanks to Håkan Gustafsson for all the time he spent introducing me to the world of lithium formate EPR dosimetry. Thanks also to the hospital physicists at Linköping Hospital; Sara Olsson, Håkan Hedtjärn, Peter Larsson as well as Emil Bengtsson at Karolinska University Hospital. Without their assistance and practical tips this study would not have been possible. Bengt Frost produced the phantom for the ^{192}Ir source. I am also grateful to Gudrun Alm Carlsson for sharing parts of her vast dosimetry knowledge with me. Finally I would like to thank Axel Israelsson for his interest in discussing stylistic aspects of my work.

8 REFERENCES

ATTIX FH, Introduction to radiological physics and radiation dosimetry, Wiley-VCH, 1986

BASTIN KT, PODGORSAK MB and THOMADSEN BR: Transit dose component of high dose rate brachytherapy: Direct measurements and clinical implications, Int. J. Radiation Oncology Biol. Phys. 26, 695-702, 1993

BERGER MJ, COURSEY JS, ZUCKER MA and CHANG J: ESTAR, PSTAR, and ASTAR: Computer Programs for Calculating Stopping-Power and Range Tables for Electrons, Protons, and Helium Ions (version 1.2.3). [Online] Available: http://physics.nist.gov/Star [2008, March 19]. National Institute of Standards and Technology, Gaithersburg, MD, 2005

BERGER MJ, HUBBELL JH SELTZER SM, CHANG J, COURSEY JS, SUKUMAR R and ZUCKER DS XCOM: Photon Cross Section Database (version 1.3). [Online] Available: http://physics.nist.gov/xcom [2008, March 19]. National Institute of Standards and Technology, Gaithersburg, MD, 2005

BERGSTRAND ES, HOLE EO and SAGSTUEN E: A Simple Method for Estimating Dose Uncertainty in ESR/Alanine Dosimetry, Appl. Radiat. Isot. Vol. 49, No. 7, 845-854, 1998

BRAHME A: Correction of a measured distribution for the finite extension of the detector, Strahlentherapie 157, 258-259, 1981

BURLIN TE: in ATTIX FH, Radiation dosimetry, Academic Press, 1968

CARLSSON TEDGREN Å: personal communication

FRODESEN AG, SKJEGGESTAD O and TOFTE H: Probability and statistics in particle physics, Universitetsforlaget, 1979

GUZMAN CALCINA CS, DE ALMEIDA A, OLIVEIRA ROCHA JR, CHEN ABREGO F and BAFFA O: Ir-192 HDR transit dose and radial dose function determination using alanine/EPR dosimetry, Phys. Med. Biol. 50, 1109-1117, 2005

GUSTAFSSON H: Development of Sensitive EPR Dosimetry Methods, Linköping University Medical Dissertations, No. 1044, 2008

HOUDEK PV, SCHWADE JG, WU X, PISCIOTTA V, FIEDLER JA, SERAGO CF, MARKOE AM, ABITBOL AA, LEWIN AA, BRAUNSCHWEIGER PG and SKLAR MD: Dose determinationo in high dose-rate brachytherapy, Int. J. Radiation Oncology Biol. Phys. 24, 795-801, 1992

HUBBELL JH and SELTZER SM Tables of X-Ray Mass Attenuation Coefficients and Mass Energy-Absorption Coefficients (version 1.4). [Online] Available: http://physics.nist.gov/xaamdi [2008, March 19]. National Institute of Standards and Technology, Gaithersburg, MD, 2004

IAEA 2000 Absorbed Dose Determination in External Beam Radiotherapy: An International Code of Practice for Dosimetry based on Standards of Absorbed Dose to Water (Technical Report Series No 398), 2000

ISO 1995 Guide to the expression of uncertainites in measurement (Geneva: ISO), 1995
MALINEN E, WALDELAND E, HOLE EO and SAGSTUEN E: The energy dependence of lithium formate EPR dosimeters for clinical electron beams. Phys. Med. Biol. 52, 4362-4369, 2007

MELI JA, MEIGOONI AS and NATH R: On the choice of phantom material for the dosimetry of Ir-192 sources. Int. J. Radiat. Oncol. Biol. Phys 14, 587-594, 1988

MOHAN R, CHUI C and LIDOFSKY L: Energy and angular distributions of photons from medical linear accelerators, Med. Phys. 12 (5), 592-597, 1985,

OREAR J: Least squares when both variables have uncertainties, Am. J. Phys. 50 (10), 912-916, 1982

RIVARD MJ, COURSEY BM, DEWERD LA, HANSON WF, HUQ MS, IBBOTT GS, MITCH MG, NATH R and WILLIAMSON JF, Update of AAPM Task Group No. 43 Report: A revised AAPM protocol for BT dose calculations, Med. Phys. 31, 633-674, 2004

THOMADSEN B R, RIVARD M J and BUTLER W M, Brachytherapy Physics, Medical Physics Publishing, 2005

THOMAS JO, TELLGREN R and ALMLÖF J: Hydrogen bond studies: XCVI. X-N map and ab initio MO-LCAOSCF calculations of the difference electron density in non-centrosymmetric lithium formate monohydrate, LiHCOO·H2O Acta Crystallogr. B 31, 1946–55, 1975

VESTAD TA, MALINEN E, LUND A, HOLE EO and SAGSTUEN E: EPR dosimetric properties of formates, Appl. Radiat. Isot. 59, 181-188, 2003

VESTAD TA, GUSTAFSSON H, LUND A, HOLE EO and SAGSTUEN E: Radiation induced radicals in lithium formate monohydrate ($LiHCO_2 \square H_2O$). EPR and ENDOR studies of X-irradiated crystal and polycrystalline samples, 2004 a

VESTAD TA, MALINEN E, OLSEN DR, HOLE EO and SAGSTUEN E:

Electron paramagnetic resonance (EPR) dosimetry using lithium formate in radiotherapy comparison with thermoluminescence (TL) dosimetry using lithium fluoride, Phys. Med. Biol. 49, 4701-4715, 2004 b

WEIL JA, BOLTON JR and WERTZ JE: Electron paramagnetic resonance, JohnWiley & Sons: New Jersey, USA, 1994

WONG TPY, FERNANDO WASANTHA, JOHNSTON PN and BUBB IF: Transit dose of an Ir-192 high dose rate brachytherapy stepping source, Phys. Med. Biol. 46, 323-331, 2001

APPENDIX

Table 13 Slab dimensions of the phantom used for dose measurements around 192Ir brachytherapy source.

Slab number	1	2	3	4	5	6	7	8
Height (cm)	2.51	2.02	2.53	2.06	2.03	2.49	2.49	2.01

Table 14 Source positions from the ^{192}Ir irradiations of Batch 1 and Batch 2. Positions are ascending upwards along z, starting at 5 and 0 cm distance from the catheter bottom respectively.

Batch 1 Brachy Vision Step size: 5 mm		**Batch 2 Nucletron Step size: 2.5 mm**	
Position	**Time (s)**	**Position**	**Time (s)**
1	8.6	1	6.1
2	75.0	2	2.2
3	50.3	3	-
4	27.9	4	-
5	41.1	5	-
6	36.0	6	2.8
7	38.8	7	8.3
8	34.5	8	14.9
9	39.2	9	21.5
10	39.9	10	28.6
11	28.0	11	34.7
12	47.8	12	39.6
13	80.6	13	43.5
14	6.0	14	45.7
-	-	15	46.8
-	-	16	46.2
-	-	17	44.0
-	-	18	41.3
-	-	19	37.4
-	-	20	33.0
-	-	21	28.6
-	-	22	24.2
-	-	23	19.8
-	-	24	16.0
-	-	25	12.7
-	-	26	9.9
-	-	27	8.3
-	-	28	7.2
-	-	29	7.2
-	-	30	7.7
-	-	31	9.4
-	-	32	11.6
-	-	33	14.9
-	-	34	18.7
-	-	35	23.1
-	-	36	27.5
-	-	37	32.5
-	-	38	36.9
-	-	39	41.8
-	-	40	45.7
-	-	41	49.5
-	-	42	51.7
-	-	43	53.9
-	-	44	55.0
-	-	45	-
-	-	46	-
-	-	47	-
-	-	48	-